September 2005 Manda Hararo-Dabbahu rifting event, Afar (Ethiopia): Constraints provided by geodetic data

R. Grandin, A. Socquet, R. Binet, Y. Klinger, E. Jacques, J.-B. de Chabalier, G C P King, C. Lasserre, S. Tait, P. Tapponnier, et al.

JOURNAL OF GEOPHYSICAL RESEARCH, VOL. 114, B08404, doi:10.1029/2008JB005843, 2009

September 2005 Manda Hararo-Dabbahu rifting event, Afar (Ethiopia): Constraints provided by geodetic data

R. Grandin,[1] A. Socquet,[1] R. Binet,[2] Y. Klinger,[1] E. Jacques,[1] J.-B. de Chabalier,[1] G. C. P. King,[1] C. Lasserre,[3] S. Tait,[4] P. Tapponnier,[1] A. Delorme,[1] and P. Pinzuti[1]

Received 1 June 2008; revised 21 March 2009; accepted 7 May 2009; published 18 August 2009.

[1] We provide a new set of complementary geodetic data for the 2005 rifting event of Afar (Ethiopia). Interferometric synthetic aperture radar and subpixel correlations of synthetic aperture radar and SPOT images allow us to deduce 3-D surface displacement unambiguously. We determine the geometry of the dike and neighboring magma chambers and invert for the distribution of opening of the dike, as well as slip on rift border faults. The volume of the 2005 dike (1.5–2.0 km^3) is not balanced by sufficient volume loss at Dabbahu and Gabho volcanoes (0.42 and 0.12 km^3, respectively). Taking into account the deflation of a suspected deep midsegment magma chamber simultaneously to dike intrusion produces a smoother opening distribution along the southern segment. Above the dike, faults slipped by an average 3 m, yielding an estimated geodetic moment of 3.5×10^{19} Nm, one order of magnitude larger than the cumulative seismic moment released during the earthquake swarm. Between Dabbahu and Ado'Ale volcanic complexes, significant opening occurred on the western side of the dike. The anomalous location of the dike at this latitude, offset to the east of the axial depression, may explain this phenomenon. A two-stage intrusion scenario is proposed, whereby rifting in the northern Manda Hararo Rift was triggered by magma upwelling in the Dabbahu area, at the northern extremity of the magmatic segment. Although vigorous dike injection occurred during the September 2005 event, the tectonic stress deficit since the previous rifting episode was not fully released, leading to further intrusions in 2006–2009.

Citation: Grandin, R., et al. (2009), September 2005 Manda Hararo-Dabbahu rifting event, Afar (Ethiopia): Constraints provided by geodetic data, *J. Geophys. Res.*, *114*, B08404, doi:10.1029/2008JB005843.

1. Introduction

[2] At mid-oceanic ridges (MOR), extension follows a magmato-tectonic cycle, with discrete episodes of intense magmatic and seismic activity separated by long periods of quiescence. During rifting episodes, the stress accumulated in the lithosphere is relieved by accretion of material, involving the injection of magma from a mantle source into one or a succession of dikes [e.g., *Björnsson*, 1985]. Dike opening at depth induces slip on steeply dipping conjugate normal faults above and perhaps ahead of the dike [e.g., *Rubin and Pollard*, 1988; *Wills and Buck*, 1997]. Migration of seismicity during the coeval earthquake swarm suggests that intrusion of an individual dike takes place within hours by lateral transport of the magma over distances that can reach several tens of kilometers [e.g., *Sykes*, 1970; *Einarsson and Brandsdóttir*, 1980; *Dziak et al.*, 2007]. Magma chamber inflation and deflation cycles can also occur when magma is temporarily trapped inside the crust prior to intrusion or extrusion [*Björnsson et al.*, 1979].

[3] Opening of dikes is largely aseismic and normal faulting contributes little to seismicity [e.g., *Solomon et al.*, 1988]. Thus, to understand the processes involved, direct observation of corifting displacements is needed. This is not possible for submarine rifts. At subaerial rifts in Iceland and Afar, direct geodetic measurements are available for only two rifting episodes (Krafla, Iceland, 1975–1984 and Asal-Ghoubbet, Djibouti, 1978).

[4] The rifting episode that is currently taking place in the Afar depression (Ethiopia), started on September 2005, provides an invaluable opportunity to constrain existing models of rifting [e.g., *Tapponnier and Francheteau*, 1978; *Lin and Parmentier*, 1990; *Buck et al.*, 2006]. This rifting episode includes a large volume dike intrusion and interaction with existing magma chambers. Conditions for satellite-based data acquisition are exceptionally good in Afar, and the static displacements at the surface were remarkably large. The deformation field can be interpreted within the

[1]Equipe de Tectonique et Mécanique de la Lithosphère, Institut de Physique du Globe de Paris, Paris, France.
[2]Laboratoire de Détection et de Géophysique, Commisariat l'Energie Atomique, Bruyères-le-Châtel, France.
[3]Laboratoire de Géophysique Interne et Tectonophysique, Université Joseph Fourier, Grenoble, France.
[4]Equipe de Dynamique des Fluides Géologiques, Institut de Physique du Globe de Paris, Paris, France.

0148-0227/09/2008JB005843$09.00

framework of the elastic rebound theory, and geodetic data may be inverted in order to retrieve the geometric parameters of the dikes and faults. *Wright et al.* [2006] and *Ayele et al.* [2007] already produced models of the slip and opening distribution. Their inversions, however, were hampered by the inherently low resolution on the predominantly E-W horizontal component of deformation, which cannot be resolved easily in the near field because of decorrelation of interferometric synthetic aperture radar (InSAR) where large rapidly changing displacements occur. Also, they did not discuss the sensitivity of their solutions to a deep deflation below the dike, which is likely to have happened.

[5] In this paper, we perform a subpixel correlation [*Michel et al.*, 1999a, 1999b] of three pairs of optical SPOT images (SPOTIO) that span the September 2005 Manda Hararo-Dabbahu rifting event. The introduction of this independent measurement of the two orthogonal components of horizontal displacement allows the rift-perpendicular horizontal component of deformation to be separated from the vertical component. Besides representing a substantial improvement in the resolution of the distribution of opening of the dike, a clearly asymmetric behavior of normal faults above the dike is documented for the first time. These new observations also have implications on our understanding of the mechanics of rupture at low confining pressure and of the accretion processes that take place at magmatic rift segments.

2. Regional Context and Overview of the Rifting Episode

2.1. Tectonic Setting

[6] The Afar triple junction lies between the diverging Nubian, Arabian and Somalian plates (Figure 1a) [e.g., *McKenzie and Davies*, 1970; *Mohr*, 1970]. It formed by stretching of the cratonic lithosphere of NE Africa, which initiated around 30 Mya in response to the regional uplift caused by the impact of a large plume [e.g., *Burke and Dewey*, 1973; *Courtillot*, 1982; *White and McKenzie*, 1989; it *Schilling et al.*, 1992; *Ebinger and Sleep*, 1998]. From around 15 Mya, sustained extension and oceanization occurred along the Red Sea and Aden ridges [e.g., *Cochran*, 1981; *Leroy et al.*, 2004; *Bosworth et al.*, 2005]. Within the Afar depression, the eruption of the mainly basaltic trapp-like Stratoid Series, between 3 Mya and 1 Mya, is generally believed to mark the onset of continental breakup [*Barberi et al.*, 1975; *Barberi and Santacroce*, 1980; *Courtillot et al.*, 1984; *Deniel et al.*, 1994; *Zumbo et al.*, 1995; *Lahitte et al.*, 2003b].

[7] The Red Sea–Gulf of Aden megastructure (NNW-SSE and WNW-ESE trend, respectively) today constitutes the southwestern boundary of the Arabian plate [*Barberi et al.*, 1972b]. In northern Afar, Quaternary extension and volcanism occur along magmatic segments typified by the Erta'Ale and Alayta axial volcanic ranges [*Tazieff et al.*, 1972; *Barberi et al.*, 1972a]. Farther south, evidence of the most recent tectono-magmatic activity occurs along the Manda Hararo and Manda Hararo-Goba'ad rifts [*CNR-CNRS Afar Team*, 1973; *Varet*, 1975]. In eastern Afar, the Asal-Ghoubbet rift (Djibouti) is the onland termination of the westward propagating Gulf of Aden oceanic ridge [*de Chabalier and Avouac*, 1994; *Manighetti et al.*, 1997; *Audin et al.*, 2001]. It is connected to the Manda Inakir volcanic rift to the north via an incipient transfer zone [e.g., *Stieltjes*, 1980; *Manighetti et al.*, 1998].

[8] The incomplete connection between the Red Sea and Gulf of Aden Rift Systems involves a complex overlap in central Afar, resulting in bookshelf faulting in the overlapping area [*Tapponnier et al.*, 1990; *Manighetti et al.*, 1998; *Audin*, 1999; *Manighetti et al.*, 2001; *Kidane et al.*, 2003]. The largest earthquakes recorded in Afar (maximum magnitude $M_S = 6.3$) occurred in this area during the 1969 Serdo and 1989 Dôbi earthquake sequences; they were not associated with magmatism [*Gouin*, 1979; *Kebede and Kulhánek*, 1989; *Jacques et al.*, 1999].

[9] Estimates of the velocity of Nubia/Arabia plate divergence, directed ~N45°E at 12°N, vary from 18 mm/a for plate kinematics models (~3 Mya time-averaged) [*Jestin et al.*, 1994; *Demets et al.*, 1994; *Chu and Gordon*, 1998] to 15 mm/a for GPS measurements [*Ruegg et al.*, 1993; *Walpersdorf et al.*, 1999; *McClusky et al.*, 2003; *Vigny et al.*, 2006]. In southern Afar, the ~E-W opening of the Northern Main Ethiopian Rift (MER) occurs at a slower velocity of 5 mm/a, as determined by both "geological" [*Jestin et al.*, 1994; *Chu and Gordon*, 1999] and geodetic methods [*Mohr*, 1978; *Bilham et al.*, 1999; *Vigny et al.*, 2006]. There, strain is localized since ~2 Mya on 10 km wide en échelon magmatic segments, testifying of an early stage of incipient "oceanic segmentation", less evolved than that of central and northern Afar rifts [*Hayward and Ebinger*, 1996; *Ebinger and Casey*, 2001; *Wolfenden et al.*, 2004].

[10] Prior to the onset of the 2005 Manda Hararo-Dabbahu rifting event, the 1978 Asal-Ghoubbet rifting episode was the only example of a tectonic and magmatic crisis associated with seafloor spreading in Afar. It was associated with a fissural basaltic eruption, fissures opening, up to 80 cm of slip on normal faults within or at the edges of the inner floor, the intrusion of basaltic magma at depth along one or two vertical dikes, and a seismic swarm that lasted for 2 months (two $M > 5$ earthquakes, maximum magnitude $m_b = 5.3$) [*Abdallah et al.*, 1979; *Ruegg et al.*, 1979; *Le Dain et al.*, 1980; *Lépine et al.*, 1980]. During the main rifting event, both reactivated and newly formed fissures and faults were observed. The geometric features of the two inferred dike planes (height of 4.5 km, lengths of 4.1 and 8.9 km, and widths of 2.1 and 4.1 m) yield an estimated volume of intruded magma of 0.2 km^3 [*Tarantola et al.*, 1979]. This is about 10 times the volume of extruded lava [*Allard and Tazieff*, 1979], thus much of the material remained in the crust.

2.2. Manda Hararo-Dabbahu Rift

[11] The September 2005 rifting event ruptured the northern part of the Manda Hararo Rift (MHR) and the eastern flank of the Dabbahu volcano [*Barberi et al.*, 1972b; *CNR-CNRS Afar Team*, 1973; *Varet*, 1975] (Figure 1b). The term "Dabbahu Rift" was introduced to describe this section of the Red Sea megastructure [*Wright et al.*, 2006]. However, petrological features of lavas erupted at Dabbahu show some analogies with that of axial volcanic ranges of Erta Ale and Alayta, although the morphology of Dabbahu volcano is more that of a strato-volcano built by the recent accumulation of silicic products [*Barberi et al.*, 1974,

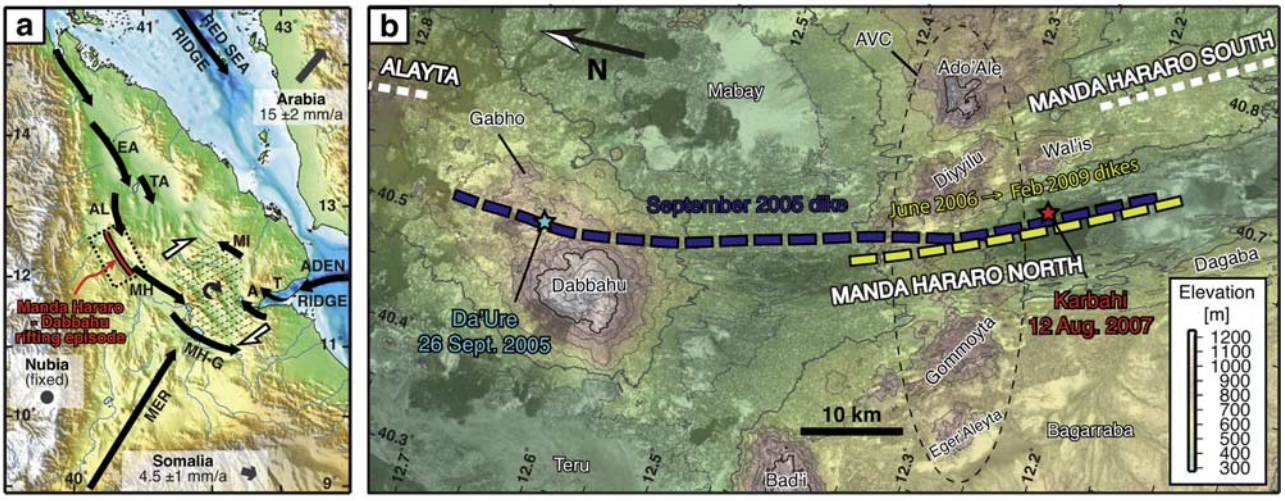

Figure 1. (a) Map of the Afar triple junction. Black arrows, rift segments with Quaternary magmatic activity (modified from *Manighetti et al.* [1998]); dashed black lines, overlap zone with bookshelf faulting [from *Tapponnier et al.*, 1990]; grey arrows, plate motion vectors [from *Vigny et al.*, 2006]; A, Asal-Ghoubbet; AL, Alayta; EA, Erta'Ale; MER, Main Ethiopian Rift; MH, Manda Hararo; MH-G, Manda Hararo Goba'Ad; MI, Manda Inakir; T, Tadjoura; and TA, Tat'Ali. (b) Topographic map of the Manda Hararo-Dabbahu Rift System superimposed on SPOT image. Toponymy after *CNR-CNRS Afar Team* [1973] and *Varet* [1975]. Stars, eruptions; white dashed lines, magmatic segments; and colored dashed lines, dikes emplaced during the Manda Hararo-Dabbahu rifting episode.

1975]. In contrast, south of Dabbahu, the northern MHR is characterized by structural and magmatic characteristics similar to that found at several second-order segments of the slow spreading Mid-Atlantic Ridge [e.g., *Lin et al.*, 1990; *Gràcia et al.*, 1999; *Dunn et al.*, 2005]. Quaternary fissural basaltic activity has taken place in the graben floor, and the axial depression is narrower and more elevated near its center, suggesting a focused midsegment melt supply [e.g., *Rowland et al.*, 2007]. Migration of seismicity during the emplacement of the June and July 2006 dikes suggests that this inferred source of magma (which we call "Wal'is magma chamber" in the following) is currently active, and has fed the dikes intruded in the MHR from 2006 to 2009 [*Keir et al.*, 2008; *Ebinger et al.*, 2008; *Hamling et al.*, 2008]. Furthermore, a now partially dissected Silicic Central Volcano, the Ado'Ale Volcanic Complex (AVC), lies on both sides of an axial basaltic shield volcano, a configuration similar to the proto-oceanic Asal-Ghoubbet Rift (Djibouti) [*de Chabalier and Avouac*, 1994; *Lahitte et al.*, 2003a], and some sectors of the Mid-Atlantic Ridge [e.g., *Rabain et al.*, 2001].

[12] In this paper, we make a distinction between (1) the "Dabbahu Volcanic Complex" (north of 12.60°N), where faults have an overall ~N-S trend, and (2) the "Northern Manda Hararo Rift" (south of 12.60°N), which has a more NNW-SSE trend and is itself divided into a northern and a southern part separated by AVC at 12.35°N. For convenience, the terms "Northern Manda Hararo" (NMHR) and "Dabbahu" are used in the following. The name "Manda Hararo-Dabbahu Rift" is preferred to the term "Dabbahu Rift".

[13] The Manda Hararo-Dabbahu Rift overlaps with the Manda Inakir Rift in its southern part only (Figure 1a); thus, we assume that, along this section of the plate boundary, extension operates at nearly the full spreading rate. The southern MHR is offset to the east with respect to the northern MHR; to the north, the Alayta volcanic range is also offset to the east (Figure 1b) [e.g., *Hayward and Ebinger*, 1996; *Manighetti et al.*, 1998; *Rowland et al.*, 2007]. Whether the existence of Dabbahu is a consequence of the relay zone between the Alayta magmatic segment and the MHR, as can be deduced from an analogy with segmentation of the northern MER, or was "captured" by the current rift zone configuration, is still debated [*Ebinger and Hayward*, 1996; *Ebinger et al.*, 2008].

2.3. Overview of the 2005 Manda Hararo-Dabbahu Rifting Event

[14] The term "2005 Manda Hararo-Dabbahu rifting event" here refers to the events that took place in this region from late September to early October 2005, while the "Manda Hararo-Dabbahu rifting episode" includes the whole series of related events that occurred from mid-September 2005 to 2009.

[15] The Manda Hararo-Dabbahu rifting event started on 14 September 2005 with a seismic swarm that lasted for about 20 days; seismic activity culminated on 24–25 September 2005, with the occurrence of the largest shock (M_w = 5.5) and the maximum number of events (Figure 2) [*Wright et al.*, 2006; *Yirgu et al.*, 2006; *Ayele et al.*, 2007]. The cumulative seismic moment of the 167 events reported by NEIC is 3.4 (±0.7) × 10^{18} Nm, equivalent to a single M_w = 6.3 earthquake (auxiliary material).[1] A total of 15 earthquakes with $M > 5$ were recorded; the 20 available CMT focal mechanisms show predominantly normal faulting [*Dziewonski et al.*, 1981], except for 4 of the largest shocks ($5.5 > M_w > 5.0$), for which the double-couple

[1] Auxiliary materials are available in the HTML. doi:10.1029/2008JB005843.

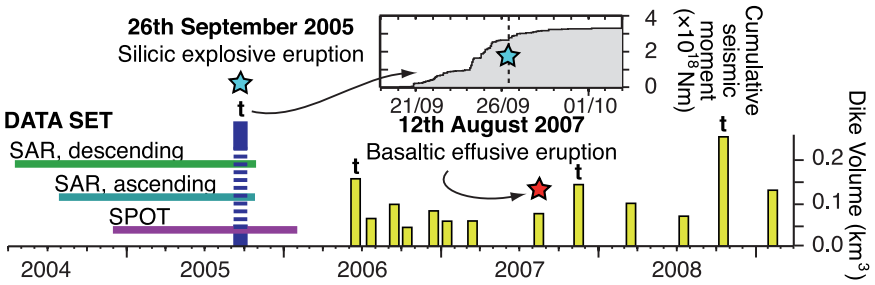

Figure 2. Timing of the main events of the Manda Hararo-Dabbahu rifting episode. Horizontal lines, time interval of geodetic data; vertical lines, dikes, with height proportional to dike volume, from a preliminary inversion of InSAR data (September 2005 dike not to scale); stars, eruptions; and t, $M > 4$ earthquakes. Inset: cumulative seismic moment released during the September 2005 earthquake swarm.

component is identified as strike slip according to the *Dziewonski et al.* [1987] decomposition. However, using the *Knopoff and Randall* [1970] decomposition for these 4 events, the double-couple component only represents 58% to 24% of the total moment.

[16] An explosive eruption occurred on 26 September 2005 at Da'Ure, a locality situated on the eastern flank of Dabbahu volcano (Figure 1b) [*Yirgu et al.*, 2006; *Ayele et al.*, 2007]. The composition of erupted material is consistent with heating of a felsic magma caused by the influx of hot basaltic material [*Wright et al.*, 2006; *Yirgu et al.*, 2006].

[17] In the Da'Ure area, one individual westward facing fault showed evidence of fresh vertical displacements of up to 5 m [*Yirgu et al.*, 2006; *Rowland et al.*, 2007]. On the northern side of the AVC, *Rowland et al.* [2007] reported extensive faulting and fissuring, with up to 6 m of dip-slip motion on a group of faults and fissures forming a small graben; in this area, dilation predominantly occurred ~2 km to the east of the inferred axial depression, which remained undisturbed. It is not known whether the large quantities of slip were accommodated at once, or accrued during several subevents.

[18] InSAR studies of the September 2005 rifting event showed that a 65 km long dike had opened by an average 4 m at 2–8 km depth, with a maximum of 8 m; ~2 m of subsidence had also occurred above two magma chambers located on either side of the eruption site, below Dabbahu and Gabho [*Wright et al.*, 2006; *Ayele et al.*, 2007]. *Wright et al.* [2006], using synthetic aperture radar (SAR) image offsets (SARIO) in addition to InSAR data, also inverted for slip on two sets of conjugate 65°-dipping normal faults above the dike; their best fit model yields an average ~2 m of slip (maximum ~7 m).

[19] Relative relocations showed that seismicity prior to 24 September 2005 predominantly occurred to the north, possibly in the Dabbahu area, while later earthquakes were located 20–30 km more to the south; however, only regional and distant stations provided data for this time period, and absolute locations are poorly constrained [*Wright et al.*, 2006; *Ayele et al.*, 2007]. Making an analogy with the Askja (1874–1875) and Krafla (1975–1984) rifting episodes in Iceland [e.g., *Sigurdsson and Sparks*, 1978; *Brandsdóttir and Einarsson*, 1979; *Tryggvason*, 1984; *Björnsson*, 1985], *Ayele et al.* [2007] suggested that an injection of magma from the northern magma chambers into the dike could not be ruled out. However, the volume loss at the two magma chambers is only ~30% of the dike volume, and alternative mechanisms have been invoked: (1) underestimation of the actual volume loss at magma chambers due to simplistic assumptions in elastic inversions, (2) undetected transit of magma into and then out of the shallow magma chambers occurring between the two SAR acquisition dates, and/or (3) deflation of a deeper, yet undetected magma chamber [*Wright et al.*, 2006; *Ayele et al.*, 2007; *Hamling et al.*, 2008].

[20] An emergency seismic network was deployed on 19 October 2005. In the few months that followed the main rifting event, the dense seismic activity at Dabbahu (which continued deflating until January 2006) and Da'Ure, and the contrasting "silent" reinflation of Gabho magma chamber, point to complex magmatic plumbing in the Dabbahu area. Continued seismicity, with normal focal mechanisms, was also measured along the newly intruded dike; yet, while faulting occurred down to 12.15°N during the September 2005 rifting event, no earthquakes could be located by the emergency network south of 12.30°N [*Ebinger et al.*, 2008].

[21] A total of ten smaller intrusion events have occurred in the southern part of the Northern Manda Hararo Rift from June 2006 to February 2009 (Figure 1b) [*Ebinger et al.*, 2008; *Keir et al.*, 2008; *Hamling et al.*, 2008]. Seismicity associated with the emplacement of the 17 June 2006 dike migrated from south to north, whereas the 25 July 2006 dike propagated toward the south; this is compatible with the presence of a midsegment magma reservoir at great depth (>10 km) [*Keir et al.*, 2008]. However, except perhaps in the case of the southernmost dike of 12 November 2007, deflation of this magma source could not be clearly deduced from geodetic data [*Hamling et al.*, 2008].

3. Data

3.1. InSAR

[22] The ENVISAT satellite of the European Space Agency has collected SAR data both before and after the September 2005 rifting event (Table 1). Using the ROI_PAC software [*Rosen et al.*, 2004], we processed two interferograms spanning the main intrusion event, on tracks 49 and 28 (descending and ascending passes, respectively) (Figures S1a and S1b). This technique provides a measurement of ground displacements projected onto the line of sight (LOS) of the satellite, which makes an ~20° angle with the vertical. The topographic signal

Table 1. Data Set Used for the Inversion

Data Set	InSAR Descending	InSAR Ascending	SARIO Range Descending	SARIO Range Ascending	SARIO Azimuth Descending	SARIO Azimuth Ascending	SPOTIO Row SE	SPOTIO Row NE	SPOTIO Row NW	SPOTIO Column SE	SPOTIO Column NE	SPOTIO C Column NW	Total
Original number of points	1347418	2713781	1595333	678321	1489605	654413	102627	144153	143561	102627	144153	143561	9259553
Downsampled number of points	1420	1500	585	556	585	555	138	126	240	138	126	240	6209
Weight (%)	22.87	24.16	9.42	8.95	9.42	8.94	2.22	2.03	3.87	2.22	2.03	3.87	100.00

was removed from the interferograms using the 3 arc sec SRTM digital elevation model (DEM). Ground pixel size is 90 m, and accuracy of measurement is of the order of magnitude of ~1 cm (Table 2). The western side of the rift is well covered by the descending track only. The coherence is excellent, and phase unwrapping was possible up to ≤2 km from the rift zone. In the inner region, large displacement gradients impeded further unwrapping.

3.2. SAR Image Offsets

[23] We correlated SAR amplitude images to measure subpixel displacement in the LOS of the satellite ("SARIO range", Figures S1c and S1d) and horizontally along the satellite heading direction ("SARIO azimuth", Figures S2a and S2b) [e.g., *Michel et al.*, 1999b]. We used the same prediking and postdiking SAR images that were used for InSAR (Table 1). Correlation is calculated on 4 (in range) by 20 (in azimuth) pixel-wide windows, yielding a SARIO ground pixel size of 90 m. The accuracy of the measurement is typically ~10% of the pixel size of the raw SAR image (~4.7 m in azimuth, ~7.8 m in slant range); thus, the error in azimuth (~30 cm) is less than the error in range (~50 cm) (Table 2). However, errors are not uniformly distributed: they are larger in the areas where InSAR coherence is low (ponds, vegetated areas), and at image edges. The measurement provided by SARIO range is complementary to InSAR, since SARIO is efficient in the regions where ground displacement is large, that is where InSAR usually decorrelates; SARIO azimuthal offsets provide information about horizontal displacements that are perpendicular to the InSAR LOS displacements.

3.3. SPOT Image Offsets

[24] Applying the subpixel correlation method to optical images [e.g., *Michel et al.*, 1999a, 1999b; *Van Puymbroeck et al.*, 2000; *Leprince et al.*, 2007], which may have a much higher resolution than SAR amplitude images, is currently the most efficient way of measuring the two horizontal components of the displacement field [e.g., *Michel and Avouac*, 2002; *Dominguez et al.*, 2003; *Klinger et al.*, 2006]. We performed a correlation of 10 m resolution SPOT-2 and SPOT-4 images (Figures 3a, S2c, and S2d). The scenes were acquired at the same hour of the day, with an approximately 1 year temporal baseline and with an incidence angle close to vertical (Tables 1 and 2). Prior to coregistration, images were first resampled to 8 m resolution to prevent information loss, and correlation was calculated on 16 pixel-wide windows, yielding a SPOTIO ground pixel size of 128 m. The two orthogonal components of the horizontal displacement are measured ("SPOTIO column" and "SPOTIO row"). In order to cover the whole rift, three image pairs were processed separately.

[25] The key problem that arises when using SPOT image offsets is the removal of two orthogonal "corrugated perturbations" of the signal with a typical wavelength > 5 km. These perturbations are caused by inaccuracies in the determination of the satellite attitude (pitching and rolling), and affect independently the measurements made along columns and rows. For each component, we removed the perturbation empirically, in an iterative fashion, by stacking measurements along one coordinate axis, then fitting the resulting stack with an appropriate polynomial function, and

Table 2. Time Intervals Covered by the Geodetic Data Presented in This Study

Data	Image Location/Type	Image A	Image B	Temporal Baseline (Days)	Perpendicular Baseline (m)	Postdiking Time Spanned (Days)
InSAR/SARIO	descending	16/04/04	28/10/05	560	30	33
	ascending	28/07/04	26/10/05	455	385	31
SPOTIO	SE	21/02/05	25/01/06	338	-	122
	NE	21/02/05	25/01/06	338	-	122
	NW	19/12/04	13/01/06	390	-	110

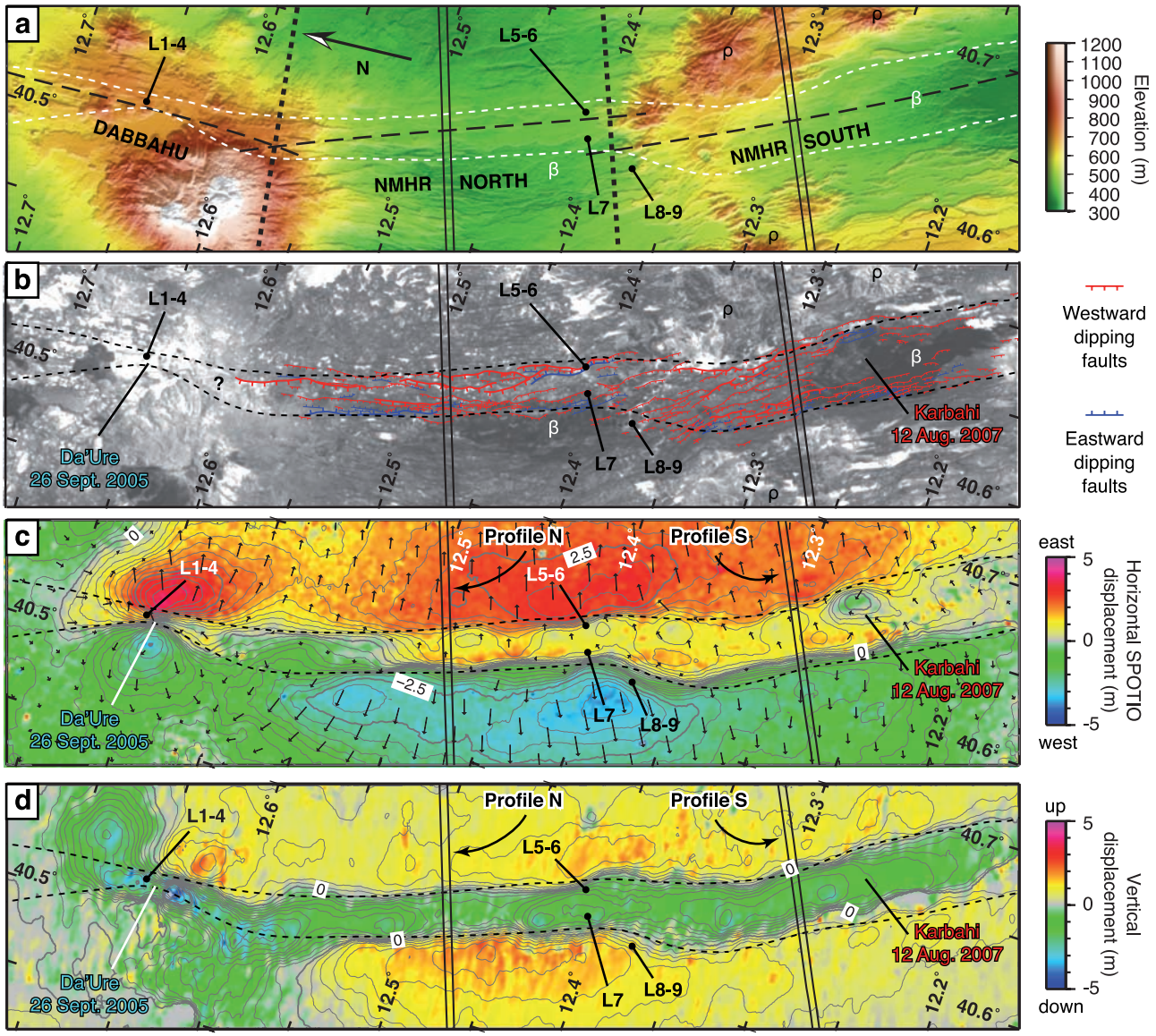

Figure 3. (a) The 20 m resolution DEM of the area. (b) Mapping of faults that were active after the main rifting event, superimposed on SPOT image. (c) Horizontal displacements measured by SPOT image correlation (SPOTIO), projected onto a direction perpendicular to the rift (N70°E); arrows show the direction and magnitude of horizontal displacements. (d) Vertical displacements deduced from SARIO, after removal of the horizontal component obtained from SPOTIO. Dots, locations of field observations described by *Rowland et al.* [2007]; blue, eastward dipping faults; red, westward dipping faults; β, young basalts; ρ, silicic edifices; curved dashed lines, surface trace of normal fault planes used in the inversion; straight dashed segments, surface trace of the three dike planes used in the inversion; and double solid lines, profiles discussed in detail throughout the text.

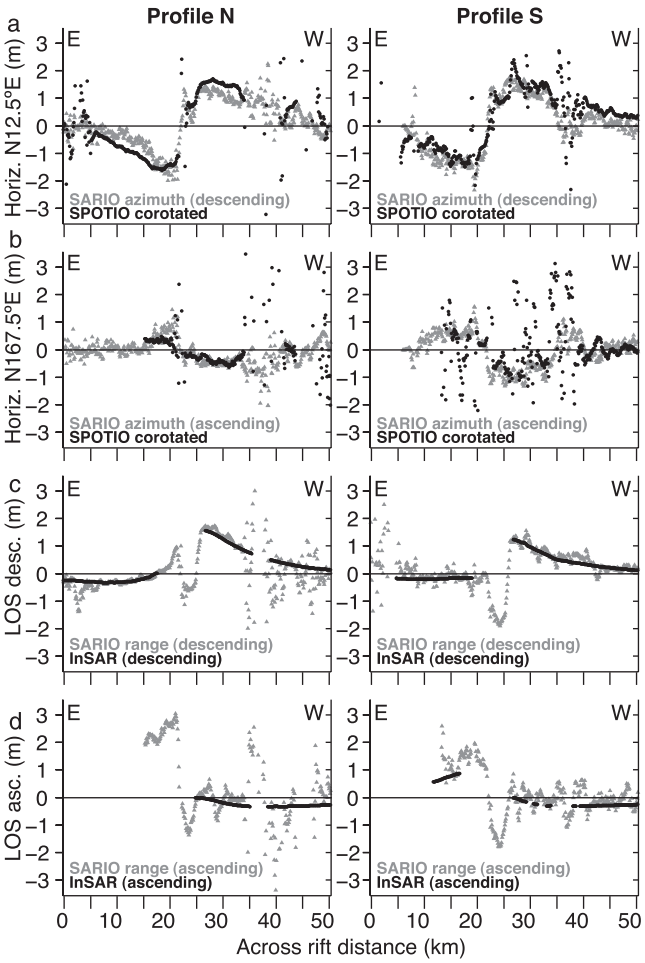

Figure 4. Comparison of the different components of surface displacement presented in this study, projected onto identical directions, at profiles (left) N and (right) S. Horizontal displacement derived from SPOTIO projected onto SARIO azimuth directions (grey) versus SARIO azimuth (black): (a) descending track and (b) ascending track. Direct comparison on LOS displacement derived from SARIO range (grey) and InSAR (black): (c) descending track and (d) ascending track. Location of profiles is shown in Figure 3.

subtracting the resulting function from the original measurement; this process is applied several times with alternating stacking directions (rows or columns), until the perturbation is removed. Prior to the fitting step, the areas of deformation were masked so that only undeformed regions were used to remove the perturbation. This process gave a very good result on two couples (SE and NE) where deformation was restricted to a small fraction of the images, and measurement errors are estimated to be less that ~30 cm at long wavelengths. On the third couple (NW) this correction was more difficult because of the presence of large areas of low correlation, and several artifacts remained superimposed on the estimated surface displacements.

3.4. Internal Consistency of the Data Set

[26] Individual image pairs do not perfectly overlap in time: SPOT scenes were acquired in early 2005 and late January 2006, and SAR-derived data integrate displacements between mid-2004 and late October 2005 (Figure 2). This is likely to introduce inconsistencies in the data set. In the prerifting period, additional InSAR images in 2004 show that deformation prior to July 2004 can be neglected. The magnitude of deformation between July 2004 and January 2005, though assumed to be small, is not known. To assess the importance of postdiking deformation occurring from late 2005 to early 2006, we processed InSAR data spanning the period between late October 2005 and early February 2006, and observed a maximum peak-to-peak cumulative LOS displacement on the descending track of ~25 cm in the southern part of the Wa'is rift, representing <10% of the observed LOS displacement associated with the 2005 rifting event. This deformation can be interpreted as continued intrusion at depth in this area [*Ebinger et al.*, 2008]. Thus, we conclude that the horizontal displacements that occurred between late October 2005 and early January 2006 are much smaller than those that occurred until late October 2005, except maybe in the vicinity of the midsegment Wal'is magma reservoir at 12.30°N, where corifting horizontal displacements detected by SPOTIO may be overestimated by up to 10% (Figure S4). In any case, although the different images presented in this paper all bracket the September 2005 event, they also include a 10 month long interval of prerifting deformation and a 1 month long interval of postdiking deformation which cannot be separated from the main rifting event.

[27] The three techniques that we used to retrieve surface displacements have distinct noise structures and individual measurements may be affected by long-wavelength biases. Fortunately, the different configurations of acquisition are geometrically redundant, allowing for cross validation of the different data sets (Table 2). For instance, the consistency of the InSAR and SARIO ranges can be readily checked, because they measure the component of the displacements projected onto exactly the same LOS vectors. Similarly, the two SARIO azimuth components on one side (ascending and descending), and the two SPOTIO components on the other side (row and column), both capture horizontal displacements on two distinct directions, allowing independent estimates of horizontal offsets along any direction. Comparisons show the very good agreement between independent observations, although some long-wavelength inconsistencies remain on the horizontal component because of an incomplete removal of column- or row-aligned perturbations of SPOTIO measurements (Figure 4). However, consistency of short-wavelength offsets, such as horizontal dilation across individual faults, is verified down to ~20 cm.

3.5. Fault Mapping

[28] Prior to interpreting geodetic data in terms of motion of faults at the surface, we mapped in detail the faults and fissures that have been active in the few months that followed the main rifting event. This was done by combining information provided by (1) panchromatic Quickbird images (resolution 60 cm), (2) a DEM generated from a pair of SPOT-5 stereo images (resolution of 20 m), (3) InSAR phase spanning the postdiking period, unwrapped at full resolution (resolution of 20 m), and (4) associated coherence image (Figure S3). For each mapped fault, using the

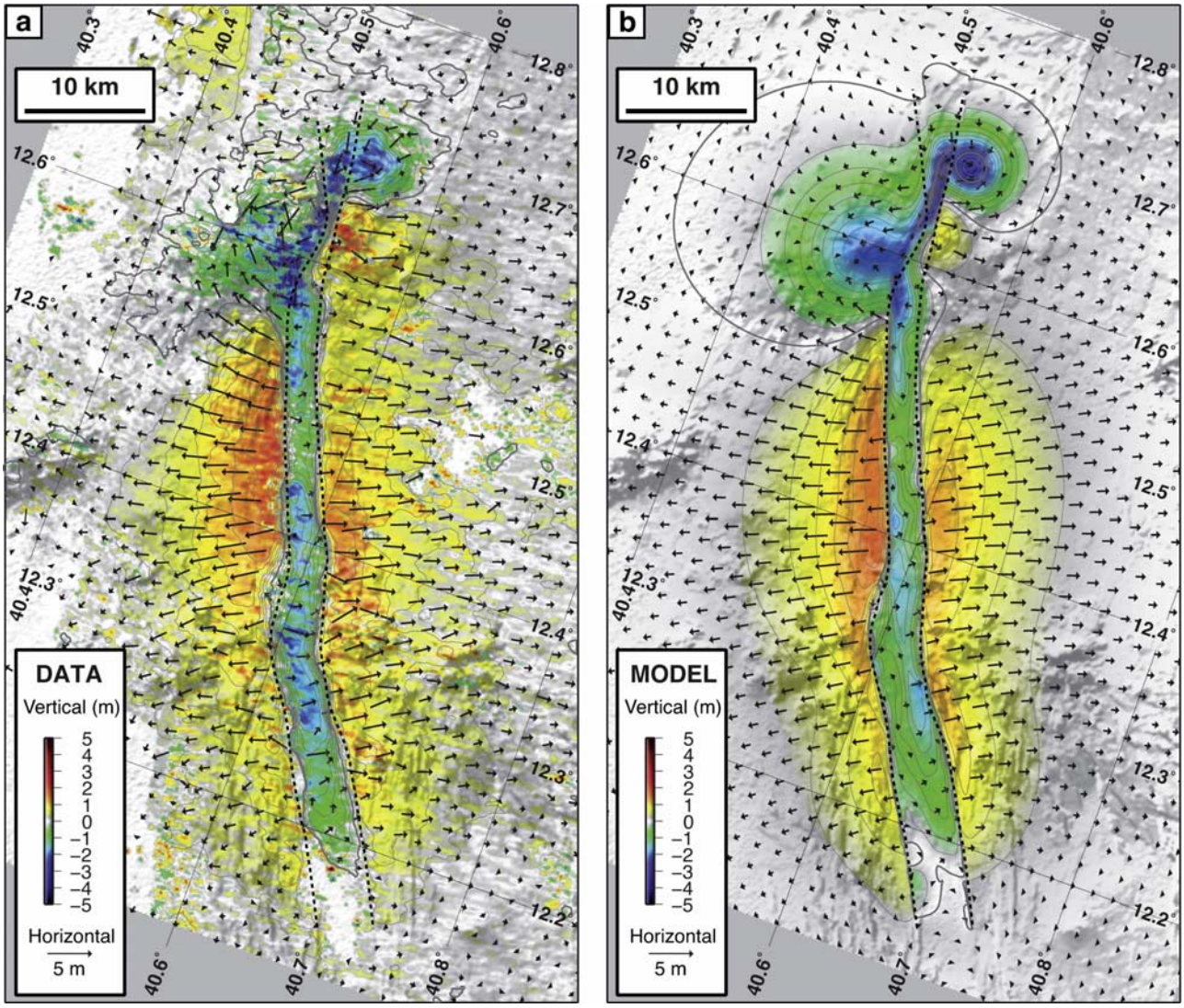

Figure 5. (a) Vertical and horizontal surface displacements deduced from a pixel-by-pixel inversion of InSAR, SARIO, and SPOTIO. (b) Modeled surface deformation, calculated with solution m2.

DEM, a dip direction was attributed (either eastward dipping or westward dipping) when the cumulative throw was sufficient. Most phase discontinuities correspond to motion on faults showing a clear topographic expression. We also mapped surface breaks associated with newly formed scarps in sediment-filled depressions and young lava flows. We have assumed that the faults for which there is clear evidence of activity after the September 2005 rifting event were also active during the rifting event itself (no newly activated structures after September 2005). No evidence of active faults breaking the surface could be observed with InSAR on the eastern slope of Dabbahu in the postdiking period (Figure S4); thus, in this area, mapping was based solely on the comparison between corifting SPOTIO measurements and fresh surface breaks observed on Quickbird images.

[29] In Figure 3, the result of this mapping has been plotted, together with the DEM derived from SPOT images, and the component of rift-perpendicular horizontal deformation during the main rifting event, deduced from SPOTIO. The observations reported by *Rowland et al.* [2007] are in agreement with the fault mapping and geodetic data presented here. In the Da'Ure area, horizontal dilation described at localities 1 to 4 reached a total of ~5 m over a lateral distance <1 km according to SPOTIO. The small grabens of localities 6 and 7 are indeed located on the intensely deformed sides of an 3 km wide subsiding axial zone. Localities 8 and 9, where no deformation was reported, lie just outside of this area of subsidence, on the footwall of inferred border faults.

[30] Larger-scale observations can also be made using our geodetic data set and fault mapping (Figure 3). At ~12.60°N, the change of trend of the rupture zone is abrupt; it could be caused by a perturbation provoked by the topographic load of Dabbahu and/or the presence of underlying magma chambers. South of Dabbahu, surface ruptures are arranged along two ~25 km long right stepping approximately parallel subsegments. The numerous en échelon faults at ~12.35°N are evidence of the localized step of the ruptured fault zone at the junction between the southern and northern subsegments. More surprisingly, we observe that most of the faults that were mapped have a dip toward

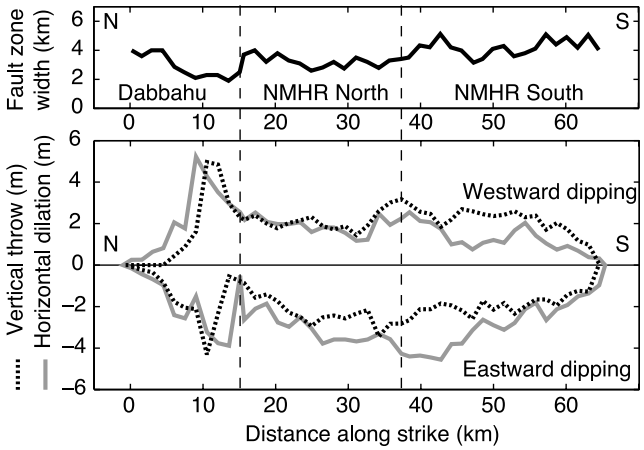

Figure 6. Graben width, vertical throw, and horizontal dilation across inferred normal faults determined at a series of locations along the dike, showing an E-W asymmetry of the amount of opening across the rift.

the west, and that only a minority of ruptured faults dip toward the east. Furthermore, the former are often associated with well-expressed scarps, while the latter have more tenuous topographic expressions. These features are most pronounced between Dabbahu and AVC; this is in keeping with the eastward position of the September 2005 dike with respect to the axial topographic low in this sector of the rift [*Rowland et al.*, 2007]. This suggests a segmentation of the rupture into three subsegments, as shown in Figure 3. We also notice a widening of the subsiding zone, from 2 km to the north, to 3 km at the center, and 4 km to the south.

3.6. Preliminary Ground Motion Analysis

[31] Our data set consists of 8 independent measurements of projected surface displacements: two InSAR (ascending and descending), two SARIO range (ascending and descending), two SARIO azimuth (ascending and descending), two SPOTIO (row and column). In most of the area of interest, accurate measurement of horizontal displacement (SPOTIO), allows for separation of the vertical and horizontal components of displacement using a simple pixel-by-pixel least squares inversion (Figure 5a). To the first order, we observe (1) horizontal displacements of the rift shoulders away from the axis, in a ENE-WSW direction, combined with uplift, (2) subsidence of the rift inner floor, and (3) subsidence in two circular regions, at the northern end of the rift. These are interpreted as the superimposed effects of (1) the inflation due to the opening of a vertical dike at depth [*Pollard et al.*, 1983], (2) dip-slip motion on shallow synthetic and antithetic normal faults located along the borders of the rift [*Rubin and Pollard*, 1988], and (3) deflation of two magma chambers [*Mogi*, 1958], respectively.

[32] Finally, in Figure 6, the vertical and horizontal offsets across the inferred border faults have been plotted along strike (estimates are not well constrained in the Dabbahu area, and will not be discussed). We observe that, south of ~12.55°N, the estimated vertical throw is fairly equally partitioned between the two sides of the dike, with an average value of ~2.5 m. However, the horizontal component of offset is systematically larger across the inferred eastward dipping border fault (~3–4 m) than across the inferred westward dipping border fault (~2 m), especially between Dabbahu and AVC. This indicates asymmetry of the motion on border faults, resulting in an absolute ~1.5 m eastward horizontal displacement of the "wedge" of crust bounded by these conjugate fault systems. This possible shallow opening on one side of the dike will be taken into account in the inversions presented in section 4.

4. Elastic Modeling: Fitting Geodetic Data With Dikes, Sills, and Faults

[33] In this section, following a linear inversion, we use surface displacements to invert for dike opening, magma chamber deflation, and slip on border faults by modeling them as dislocations in an elastic half space [*Okada*, 1985]. The final solution is not unique, and relies on a series of assumptions: data downsampling (decimation), geometry and discretization of the model, and regularization parameters.

4.1. Data Decimation

[34] Decimation must be performed in order to keep the inverse problem computationally tractable. Subsampling cannot be too severe in the near field because of strong gradients of deformation. On the contrary, far-field data are highly redundant, because of a lower gradient of deformation, but must still be taken into account because it contains information on deep processes. Building a resampled data set with a spatially variable sampling density is the best method to achieve this task [e.g., *Jónsson et al.*, 2002; *Simons et al.*, 2002; *Lohman and Simons*, 2005]. In this study, we have implemented a scheme whereby sampling density of each data set is decreased incrementally as distance from the fault zone increases (Figure S6). We also forced the relative sampling density of every component to remain uniform. Thus, the resampled data set contains more points close to the rift, and each measured component everywhere represents the same fraction of the data subset. After this subsampling step, no further weighting is performed, and all points have the same weight in the inversion. From an initial number of 9.3×10^6 pixels, the data subset is reduced to 6.2×10^3 points (Table 3).

4.2. Model Geometry

4.2.1. Dike Geometry

[35] Prior to the inversion of the whole data set, we determined the position and the geometry of the dike at depth using a nonlinear inversion scheme [*Tarantola and Valette*, 1982]. For this step, following *Rubin and Pollard* [1988], near-field data (within 4 km from the border faults) was masked, to exclude the deformation induced by normal faulting. The part of the data set that is less biased by long-wavelength perturbations has been used (the 2 InSAR images, plus SARIO azimuth for the descending orbit). Modeling far-field data requires three dike planes, and two deflating magma chambers (Figure S7). The RMS misfit (40 cm) represents ~17% of maximum displacement in the data subset (~240 cm). Average opening reaches 4.5 m, and is deepest along the northern part of the Northern Manda Hararo Rift. At Dabbahu, the best fit is obtained with a steeply eastward dipping dike (78°E). Magma

Table 3. Geometric Features of the Various Components of Displacement Measured by InSAR, SARIO, and SPOTIO, and Associated Errors

Data set	InSAR Descending	InSAR Ascending	SARIO Range Descending	SARIO Range Ascending	SARIO Azimuth Descending	SARIO Azimuth Ascending	SPOTIO Row	SPOTIO Column
Typical measurement error	1 cm	1 cm	50 cm	50 cm	30 cm	30 cm	20–100 cm[a]	20–100 cm[a]
Azimuth (clockwise, with respect to north)	102.5°	257.5°	102.5°	257.5°	192.5°	347.5°	188.0°	278.0°
Incidence angle (with respect to vertical)	22°	18°	22°	18°	90°	90°	85–90°	85–90°
Projection vector								
E-W	0.359	−0.270	0.359	−0.270	0.216	0.216	0.988	−0.153
N-S	−0.079	−0.059	−0.079	−0.059	0.976	−0.976	−0.153	−0.988
U-D	0.932	0.961	0.932	0.961	0.000	0.000	0.000	0.000

[a]Depending on the spatial wavelength of the signal (see text for discussion).

chambers are modeled as 1 km^2 square-shaped horizontal cracks, similar to sill-like point sources. We obtain magma chamber depths of 9 km at Dabbahu and 4 km at Gabho. However, using Mogi-like sources instead of sill-like sources would decrease the inverted magma chamber depths by ~25% [*Fialko et al.*, 2001]; keeping this in mind, our estimate is in good agreement with the depth of the cluster of seismicity at 5 km depth below Dabbahu determined by *Ebinger et al.* [2008].

[36] The geometry of the 3 dike planes and 2 magma chambers will be fixed in the following to estimate the opening distribution along the dike. The dike plane is discretized into a series of patches 2 km long along strike, and 10 patches along dip (0.5 km width down to 1 km depth, 1 km width down to 4 km depth, 2 km width down to 10 km depth, 4 km width down to 18 km depth). The size of the patches is a compromise between expected accuracy and computational cost. The increase of patch width at depth reflects the decreasing resolution on dike opening at increasing depths [e.g., *Lohman and Simons*, 2005].

4.2.2. Faults Geometry

[37] The mapping described in section 3.5 is used to define the location of two conjugate normal faults in the model. The horizontal position of the two fault planes has been carefully adjusted in order to match with the two zones where the maximum gradients of deformation are observed at the surface (Figure 4). Fault planes are divided in 2 km long patches along strike (40 for eastward dipping faults, 39 for westward dipping faults), and four patches along dip (two patches down to 1 km depth and two patches between 1 and 3 km depth, where they nearly intersect the dike planes). Patches have been intentionally included beyond the southern and northern limits of the fault zone to check whether inverted slip correctly tapers at the extremities of the rift. We assume that all faults have a dip of 65°, a value compatible with active normal faults in magmatic rifts of Afar [e.g., *Stein et al.*, 1991; *Manighetti et al.*, 1998]. However, as shown in section 3.6, their kinematic behavior may depart from pure dip slip; thus, opening is also allowed on fault planes in a second inversion. Strike slip is not allowed.

4.3. Inversion Method

[38] We use a least squares inversion method, with a nonnegativity constraint to prevent the inversion from producing a negative opening of the dike, or reverse faulting. A minimization of the second spatial derivative of the distribution of opening and slip is also imposed as a constraint in the inversion [*Menke*, 1989]; hence, the "roughness" of the solution is controlled by a single smoothing parameter λ [*Jónsson et al.*, 2002]. This constraint is applied independently to each of the three dike planes, as well as on each of the two fault planes. This means that the opening distribution of an individual dike plane is forced to remain smooth, but is not explicitly linked to the opening or slip distribution on other dike or fault planes; overlaps are thus allowed in the inversion if the data require it. We also forced the opening to vanish below 14 km depth. Finally, we invert for a constant offset on each of the 12 data sets. Two models have been tested: when opening on fault planes is not allowed and when it is allowed. A third model including an hypothetical deflation of a midsegment magma reservoir at ~12.30°N, and providing a very different solution for the opening distribution of the dike, is discussed in section 4.4.4.

4.4. Results

[39] For low values of the smoothing parameter λ, we obtain extremely rough solutions, which do not bear any physical significance. On the contrary, overly high values of λ force the slip/opening distribution to become increasingly uniform, at the expense of the fit to the data. A reasonable

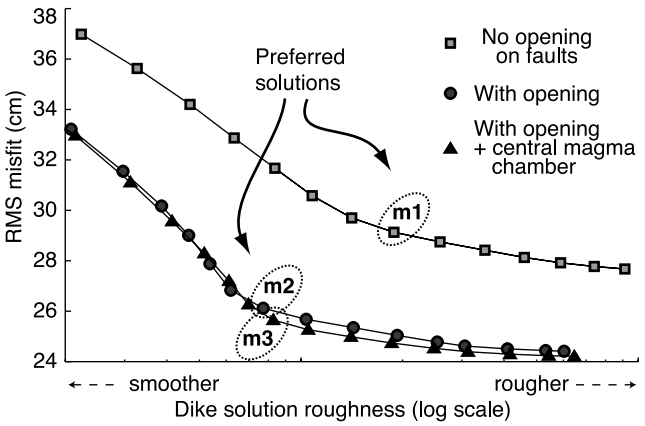

Figure 7. Computed value of the roughness of the distribution of opening on the dike [e.g., *Jónsson et al.*, 2002] versus L2 norm of misfit, as a function of the magnitude of the smoothing parameter λ.

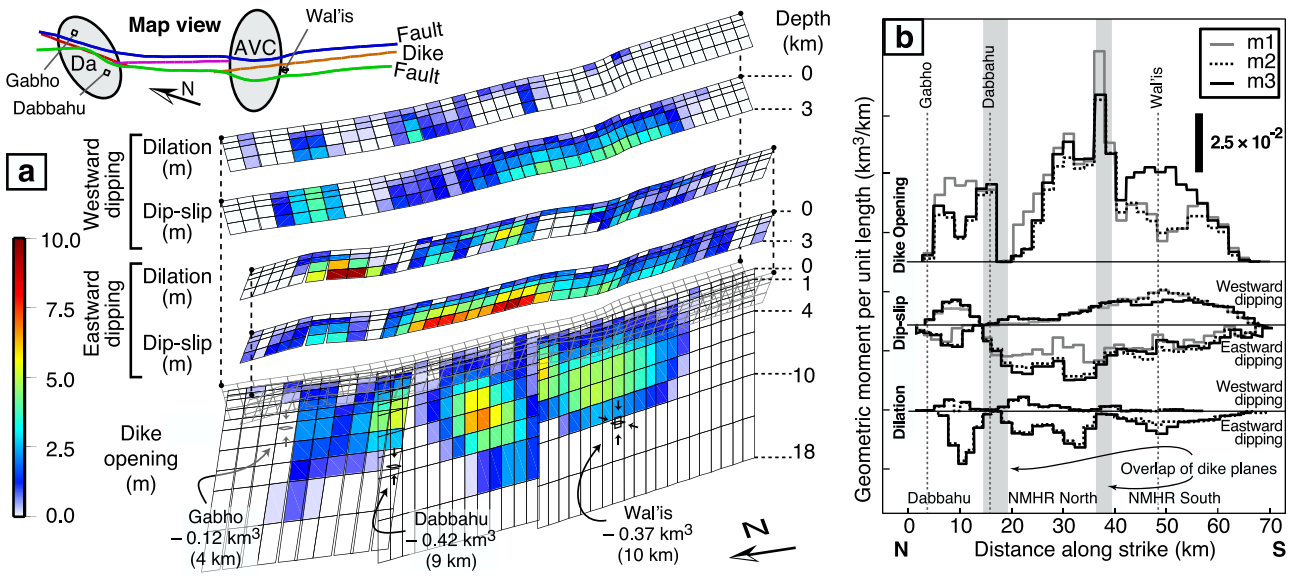

Figure 8. (a) Opening and slip distribution obtained for solution m3. Faults have been offset vertically for clarity. Solutions m1 and m2 are plotted in Figure S8 for comparison. (b) Distribution of the geometric moment released during the 2005 rifting event along strike, for solutions m1 (no opening on fault planes), m2 (opening allowed), and m3 (opening allowed, deflation of the Wal'is magma chamber).

compromise between these two end-members is found at the corner of the curve obtained by plotting the L2 norm of misfit versus solution roughness (Figure 7) [*Jónsson et al.*, 2002]. The preferred solution when only dip slip is allowed on normal faults yields a RMS of 29 cm (solution m1); when opening is allowed on fault planes too, the RMS drops to 26 cm (solution m2). The improvement of the fit from model m1 to model m2 reflects the importance of dilation at shallow depth on eastward dipping fault planes, as was shown in section 3.5.

[40] The displacement field produced by solution m2 is shown in Figure 5b. The opening and slip distribution for solution m2 is shown in Figure S8b. Three distinct zones can be outlined, which correlate spatially with the three previously identified segments: (1) the eastern slope of Dabbahu, (2) the northern part of the Northern Manda Hararo Rift, and (3) the southern part of the Northern Manda Hararo Rift.

4.4.1. Dike Planes

[41] We find that 5 m of opening occur on the dike plane close to the Dabbahu magma chamber, at ~5 km depth (Figure 8a). This zone of opening seems to connect at depth with a larger opening patch farther south, which extends down to a depth of ~14 km. A total of ~10 m opening occurs at ~4 km depth at the location where the two southern dike planes overlap. To the south, smaller values of opening are obtained, with an average 2.5 m down to a depth of ~9 km. Opening vanishes at a depth of ~1 km.

4.4.2. Dip Slip on Fault Planes

[42] In the Dabbahu area, both solutions m1 and m2 produce slightly larger amounts of slip on faults dipping toward the west, with a maximum of ~5 m occurring at the Da'Ure eruptive vent. This is in good agreement with field observations of a total of 5 m of fresh vertical offset at this location [*Rowland et al.*, 2007]. Between Dabbahu and AVC, slip is systematically larger on eastward dipping faults (>3 m) than westward dipping faults (<1.5 m). South of AVC, we obtain a smooth transition toward a more balanced repartition of slip, with ~2.5 m on either side of the fault zone (Figure 8b).

4.4.3. Dilation on Fault Planes

[43] In the vicinity of the Da'Ure eruptive vent, opening on the dike plane in solution m1 is transferred to the eastward dipping plane in solution m2, suggesting that opening is very shallow in this area, with a peak of nearly 8 m occurring at 3 km depth. Along the northern part of the Northern Manda Hararo Rift, the strong asymmetry of slip on normal faults in solution m1 is maintained in solution m2, where both slip and dilation are significantly larger on the eastward dipping fault planes. This may account for the exceptionally strong dilational component observed in the field by *Rowland et al.* [2007] on the western side of the dike at 12.40°N (Locality 7, see Figure 3). South of AVC, moderate dilation occurs on eastward dipping fault planes. Dilation on westward dipping fault planes is everywhere small, suggesting a nearly pure dip-slip behavior of faults on the eastern side of the fault zone.

4.4.4. Geometric Moment Release

[44] The geometric moment [*King*, 1978; *Ben-Menahem and Singh*, 1981], defined as the product of the area of a dislocation element (a patch in our model) by the displacement on this element (given by the solution), provides a unified way of comparing the energy release by dike opening, fault dip slip, and magma chamber deflation. The along-strike distribution of geometric moment for solution m2 is plotted in Figure 8b; solution m1 is plotted for comparison. For solution m2, 45% of the total geometric moment is released by dike opening, 40% by dip slip on normal faults, and 15% by dilation on fault planes (Figure 5b).

[45] Dip-slip motion on normal faults corresponds to 1.2 km^3 (of which 61% is released on eastward dipping faults). Assuming a modulus of rigidity of 3×10^{10} Pa, the total amount of slip on modeled faults is equivalent to a

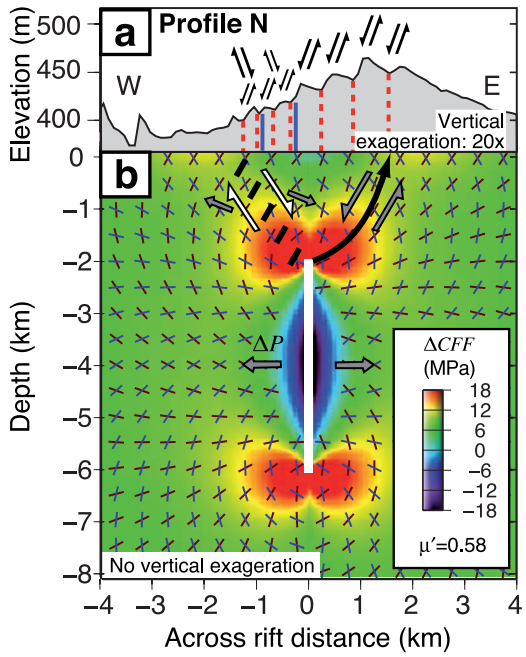

Figure 9. (a) Rift topography and location of mapped active normal faults at profile N. Red dashed lines, eastward dipping faults; and blue lines, westward dipping faults. (b) Coulomb stress change induced by the opening of the vertical dike (maximum driving stress ΔP_{max} = 40 MPa).

seismic moment release of 3.5×10^{19} Nm, which is the amount of energy released during a single M_w = 7.0 earthquake [*Hanks and Kanamori*, 1979]. This is nearly one order of magnitude larger than the cumulative seismic moment released during the September 2005 earthquake swarm (3.4×10^{18} Nm, see Figure 2 and the auxiliary material). This discrepancy appears to be ubiquitous in volcanic rift zones [*Brandsdóttir and Einarsson*, 1979; *Solomon et al.*, 1988; *Parsons and Thompson*, 1991; *Stein et al.*, 1991; *Wright et al.*, 2006; *Doubre and Peltzer*, 2007; *Keir et al.*, 2008].

[46] For the dike, the geometric moment equals its volume, which allows simple volume balances to be made. The volume increase reaches 1.30 km^3 for the dike, and 0.45 km^3 for dilation on fault planes (of which 81% occurs on eastward dipping fault planes). Compared to the results of *Wright et al.* [2006], the difference in the estimation of volume loss below Dabbahu (0.42 km^3 versus 0.3 km^3) and Gabho (0.12 km^3 versus 0.2 km^3) may arise from a different choice on the depth of the sources in the two models; yet, the total deflation is essentially the same (∼0.5 km^3). The volume of the shallow dike below the eastern flank of Dabbahu accounts for ∼0.4 km^3, which is nearly equal to the total volume loss at Dabbahu and Gabho magma chambers.

[47] The volume of magma emplaced along the Northern Manda Hararo Rift (∼1.0–1.5 km^3) corresponds to a net volume increase, for which we could not identify any corresponding deflation, probably because the magma source is too deep. In solution m2, opening of the dike at depth was greatest north of AVC, and was smaller south of AVC, a configuration similar to that found by *Wright et al.* [2006] and *Ayele et al.* [2007]. The area of opening deficit south of AVC roughly corresponds to the location of dike intrusions of 2006–2009 [*Hamling et al.*, 2008].

[48] However, the poor resolution at depth makes the solution extremely dependent on the assumptions made regarding the nature and geometry of sources of deformation at great depth. In particular, deflation of a deep magma chamber coeval to dike intrusion and fault slip would induce a widespread subsidence that would significantly bias our solutions if it is not taken into account. In a third inversion, we build on recent evidence for the presence of a >10 km deep magma reservoir (the "Wal'is magma chamber") at ∼12.30°N [*Ebinger et al.*, 2008; *Keir et al.*, 2008; *Hamling et al.*, 2008]; this modeling is not aimed at providing new insights on this deep magma reservoir, but rather is intended to highlight the influence of a deflation at great depth on the opening distribution on the dike plane at shallower depth.

[49] In this third model, the Wal'is magma chamber is modeled as a deflating composite sill/dike at 10 km depth; the choice of a greater depth and/or a different Mogi or sill-like geometry does not change our conclusions. The RMS misfit is only slightly smaller than that of the second model, showing that this additional source of deformation cannot be unambiguously detected with our geodetic data set (Figure 7). On the basis of these assumptions, the best solution (m3) yields a 0.37 km^3 deflation of the Wal'is magma reservoir. At this location, the gap in the opening of the dike disappears, and ∼5 m of opening occur between 1 km and 10 km depth. Compared to the result of *Wright et al.* [2006], which is roughly reproduced in our solution m2, our solution m3 yields a greater dike opening in the vicinity of the Wal'is magma chamber (at 50 km along strike); yet, the total volume of the dike reported by *Wright et al.* [2006] (2.5 km^3) is greater than our estimate (2.05 km^3), because of extreme dilation at depth in the Dabbahu segment in their solution (∼10 m). We conclude that the gap of opening south of AVC identified by *Wright et al.* [2006] may possibly be explained by a deep source of deflation at ∼12.30°N not taken into account in the model geometry. More observations covering subsequent rifting events in 2006–2009 will be needed to provide better constraints in identifying this potential deep magma reservoir. In contrast, the distribution of slip and opening on fault planes is unaffected by this additional degree of freedom, and is well resolved by the data. Compared to solution m2, the slip profile on faults along the dike south of AVC seems to be in better agreement with the opening distribution on the dike in solution m3, with a maximum at the latitude of the Wal'is magma reservoir, where the dike thickness reaches a local maximum (Figure 8b). This may reinforce the reliability of solution m3.

5. Boundary Element Modeling: Asymmetric Behavior of Border Faults

[50] In section 3.6, we showed that our data set documents an asymmetry in the kinematic behavior of normal faults. In section 4, we quantified the partitioning of motion on each side of the dike, and confirmed the strong component of dilation at shallow depth. However, the observation of a different dip for the faults lying on the two sides of the dike made in section 3.5 was not taken into account in the

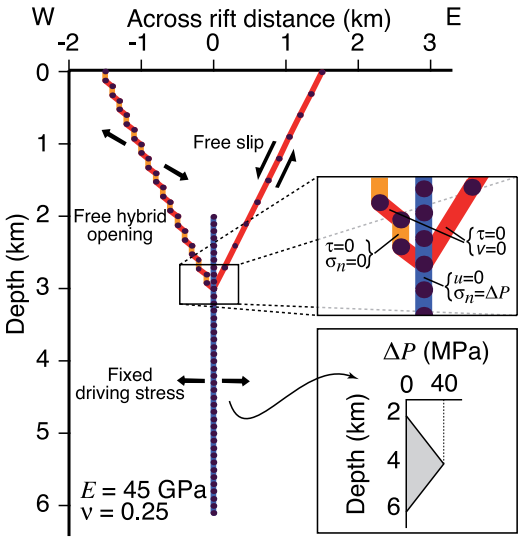

Figure 10. Conditions imposed on dislocation elements for asymmetrical modeling with the Boundary Element Method (BEM): u and v, tangential and normal displacement conditions; τ and σ_n, tangential and normal stress conditions; ΔP, driving stress; E, Young's modulus; and ν, Poisson's ratio.

inversions. In this section, we wish to reconcile these observations by investigating whether the presence of preexisting westward dipping dislocations above the dike may be responsible for asymmetric deformation at the surface. For this purpose, we use a Boundary Element Method [*Crouch and Starfield*, 1983] to fit, by forward modeling, surface displacements derived from our data set using a more complicated, perhaps more realistic, fault geometry.

[51] We focus on the two profiles located across the northern and southern parts of the Northern Manda Hararo Rift, respectively (Figure 3). The modeling is limited to two dimensions, which is valid in the near field only. The medium is modeled as a homogeneous, stress-free, isotropic, linear elastic half space. For each element, either displacement or stress boundary conditions must be imposed for directions both normal and tangential to the element (two conditions per element). The dike is modeled as a vertical crack subject to a specified triangular-shaped "driving stress", defined as the difference between magma pressure and tectonic stress orthogonal to the dike [*Pollard et al.*, 1983; *Rubin and Pollard*, 1988]. Zero shear displacement is imposed on the dike. In this simple model, the bottom depth of the dike is not constrained, because of the trade-off between dike bottom depth and the intensity of driving pressure.

[52] In Figure 9, the Coulomb Stress induced by the opening of this vertical crack, resolved on optimally oriented faults, is shown. Crosses indicate the two directions of conjugate planes on which tendency for mode II failure is maximal, based on a coefficient of friction of 0.58 [*Rubin and Pollard*, 1988; *King et al.*, 1994; *King and Cocco*, 2001]. This picture is little altered by the introduction of a preexisting extensional stress field, which we assume is of low intensity with regard to the stress concentration induced by the opening of the dike. This hypothesis may be supported by models suggesting that magma-assisted rifting occurs at a much lower deviatoric stress than tectonic rifting [e.g., *Buck*, 2006], and by the overall low background seismicity in Afar, which reflects the state of stress in the brittle part of the lithosphere [*Rubin and Gillard*, 1998].

[53] The stress field induced by dike opening at depth favors the formation of two shear zones above the crack tip [*Pollard et al.*, 1983]. Placing conjugate dip-slip faults above the modeled dike has allowed a successful modeling of the vertical deformation measured during previous rifting events [*Rubin and Pollard*, 1988; *Rubin*, 1992; *Du and Aydin*, 1992]. However, this implicitly assumes the preexistence of such faults, which does not seem to be valid on the western side of the dike intruded in 2005 between AVC and Dabbahu (see section 3.5). Our modeling strategy is different: an asymmetry is introduced by changing the kinematic behavior of the eastward dipping fault in order to increase the horizontal component of motion. This is done by dividing the eastward dipping fault into a series of linked subvertical free slipping, free opening dislocations (orange elements in Figure 10), and shallow-dipping free slipping dislocations (red elements in Figure 10). Steep free slipping, free opening dislocations represent the preexisting westward dipping faults that are unclamped by the opening of the dike; their dip can be arbitrary. The dip of the shallow-dipping free slipping dislocations controls the ratio of tangential versus normal displacement across the composite fault. They may represent newly formed ruptures that connect these preexisting defects. The resulting "fault" has a hybrid opening: it is geometrically equivalent to a 60° dipping fault and is kinematically equivalent to a fault dipping at shallower angle.

[54] The result of this asymmetrical modeling of surface deformation is shown in Figure 11; a symmetrical solution [e.g., *Rubin and Pollard*, 1988], as well as displacements deduced from solution m2 (see section 4) are shown for comparison. In the asymmetrical modeling, a good fit to the data is obtained with "kinematic" dip values of the eastward dipping fault of 39° for the northern profile, and 48° for the southern profile. On the other side of the dike, westward dipping faults dip at 60°, with pure dip-slip motion. Models involving pure dip-slip normal faults only (no hybrid opening) dipping at ~40° on the western side of the dike and ~60° on the eastern side, with a connection at ~1.5 km depth, would give almost identical results. However, such low dips seem unlikely in view of available field observations on normal faults in similar rifting contexts (see section 6 for a discussion). In this modeling, westward dipping faults have a significantly reduced slip, compared to the symmetrical model, but the balance of vertical throw on either side of the dike is preserved. This might indicate that, independently of the mechanism invoked to explain shallow dilation, the necessity of maintaining a symmetry of vertical displacements across the rift may exert a primary control on the amount of extension accommodated across each conjugate set of faults.

6. Discussion

6.1. Rifting Process at an Accreting Plate Boundary

[55] Although oceanization is still at an incipient stage in Afar, the Northern Manda Hararo Rift segment, with a ~10 km wide, ~50 km long median valley and its own central magma supply, is morphologically and magmatically

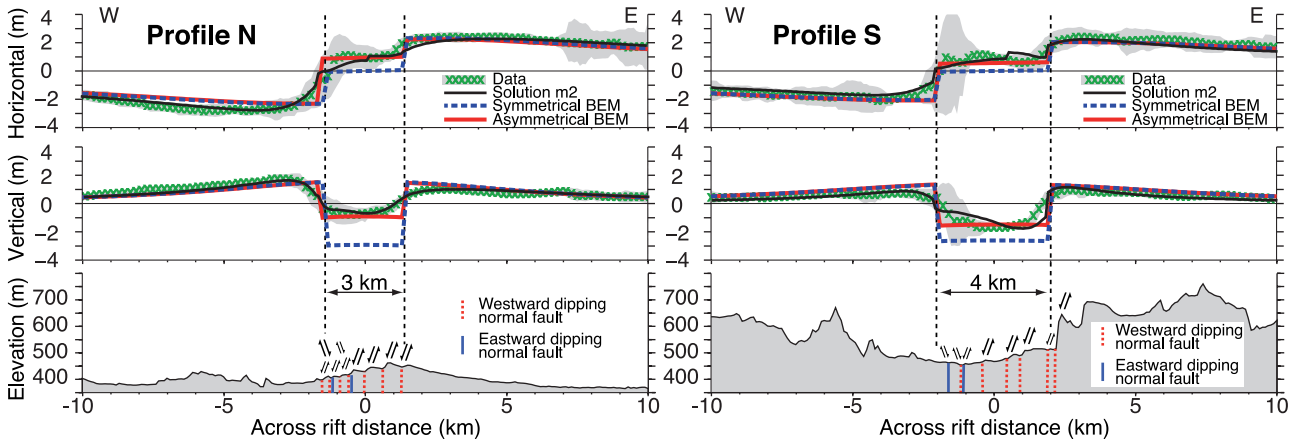

Figure 11. Comparison between the (top) horizontal and (middle) vertical displacements deduced from the geodetic data (green crosses), modeled from solution m2 (thinner line), and obtained by BEM forward modeling in a symmetrical (thick dashed line) and asymmetrical configuration (thick red line). (bottom) Same as Figure 9a.

an analogue for second-order segments of slow spreading MOR [e.g., *Ebinger and Hayward*, 1996]. Rifting episodes similar to the current Manda Hararo-Dabbahu episode have also been observed in the hot spot–influenced Northern Volcanic Zone of Iceland (Krafla, Askja), where the brittle crust thickness and spreading rate are similar to Manda Hararo. Rifting in Asal-Ghoubbet (Afar) in 1978 provided another example of a dike intrusion event at an incipient MOR segment. However, on the basis of available observations, comparison with previous events is complicated by the presence of several magma reservoirs that contributed to feeding the September 2005 dikes, and by the asymmetry of both incremental deformation and topography along the northern part of the Northern Manda Hararo Rift segment, two features that have not been observed elsewhere. In this discussion, we focus on the southern part of the Northern Manda Hararo segment, where the dike was emplaced within the axial depression.

[56] The September 2005 Manda Hararo-Dabbahu rifting event demonstrates that dikes can be emplaced, in less than two weeks, by lateral injection over distances of 25–50 km kilometers, without coeval eruption of basaltic lava. The volume of the dike intruded at Manda Hararo-Dabbahu in September 2005 ($\sim$1–2 km^3) is approximately 2 to 10 times larger than the volume of the largest and first dike of the Krafla rifting episode, in December 1975 ($\sim$0.1–0.5 km^3 [*Tryggvason*, 1984]), and is 5 to 10 times larger than the dikes emplaced in the Asal-Ghoubbet rift (Djibouti) in November 1978 ($\sim$0.2 km^3 [*Tarantola et al.*, 1979]). Theoretical studies have shown that the dynamics of dike emplacement is controlled through time by the interplay of parameters driving magma injection (magma pressure balance and deviatoric stress), parameters acting against magma injection (viscous dissipation along the dike, reduction of dike section due to freezing along dike walls), and parameters limiting the velocity of crack propagation (energy spent in advancing the process zone, viscous resistance of flow of magma into the tip region, freezing of the dike tip, pressure drop as dike lengthens) [*Weertman*, 1971; *Spence and Turcotte*, 1985; *Bruce and Huppert*, 1989; *Lister and Kerr*, 1991; *Fialko and Rubin*, 1998]. Another approach interprets the topographic lows at segment extremities as "potential wells" that drive lateral dike propagation, and attract the first dikes that escape from the central magma supply [e.g., *Tryggvason*, 1984; *Buck et al.*, 2006]. However, in September 2005, maximum opening of the dike occurred around the segment center, where altitude is not minimal, and intrusion did not propagate down to the depression located south of $\sim$12.15°N, suggesting that the along-axis slope is not the factor controlling dike emplacement.

[57] A simpler point of view, which ignores these complexities, states that maximum opening during a dike intrusion is, to the first order, controlled by the amount of driving stress along the rift segment, with this stress, on average, depending on the time interval since the previous event. At segment extremities, where overlap with nearby segments usually occurs, dikes may be arrested by the "stress shadow" induced by recent rifting activity on the other segment [*Björnsson*, 1985]. Opening during the September 2005 rifting event ($\sim$5 m), and spreading rate at Northern Manda Hararo (10–20 mm/a) [*Vigny et al.*, 2006], yield a recurrence time of 250–500 years for similar rifting episodes; this is a lower bound, as the total amount of opening will not be reached before the end of the episode.

[58] Such a long recurrence time implies a high level of accumulated elastic strain at the time of rifting initiation, hence a low ratio of effective modulus to effective failure stress (or strain to failure strain) [e.g., *Gudmundsson*, 1990]. The thick brittle crust at Manda Hararo ($\sim$8–10 km, as inferred from the depth of earthquakes [*Ebinger et al.*, 2008] and the maximum depth of dike intrusion in 2005 [*Wright et al.*, 2006; *Ayele et al.*, 2007]) may explain the high strength of the crust there. Another factor pointing to a strong crust is the absence of a shallow magma chamber at the center of the rift, which would weaken the brittle lithosphere, inducing more frequent rifting episodes [*Björnsson*, 1985; *Gudmundsson*, 1990; *Takada*, 1989]. The magma reservoir that fed the bulk of the dike in the southern part of the Northern Manda Hararo segment was probably deeper than 10 km, lacking clear expression in the geodetic data (see section 4). For comparison, the dike-

feeding Krafla magma chamber is 3 km deep [*Tryggvason*, 1986], the Asal-Ghoubbet central magma chamber is 3–5 km deep [*Doubre et al.*, 2007], and the roof of the several central magma reservoirs of the Mid-Atlantic Ridge lie at ~3–4 km [*Smith and Cann*, 1999; *Rabain et al.*, 2001; *Dunn et al.*, 2005; *Singh et al.*, 2006].

[59] Yet, one important point is that plate separation did not occur in a single dike injection at Manda Hararo and Krafla, as residual tectonic strain is accommodated by subsequent rifting events [*Arnott and Foulger*, 1994; *Hamling et al.*, 2008]. Besides confirming that the width of the dikes is limited by the amount of magma available at the onset of rifting [*Rubin*, 1992; *Qin and Buck*, 2008], this possibly allows to place an upper bound to the size of the feeding magma chamber [*Ida*, 1999]. However, in order to allow repeated rupture of the roof of the magma reservoir despite the progressive decrease of tectonic stress caused by successive intrusions, a mechanism to rapidly build up the pressure in the feeding magma system is required between intrusion events [*Einarsson and Brandsdóttir*, 1980; *Tryggvason*, 1984; *Buck et al.*, 2006]. Such mechanism has yet to be understood.

[60] An "active" type of rifting may be represented by the massive 1783–1785 Laki episode (Iceland). There, a copious fissural eruption (~15 km^3) may have been sourced directly from a large subcrustal (~10 km deep) overpressured reservoir, possibly implying very long recurrence times [*Gudmundsson*, 1987; *Sigmarssson et al.*, 1991; *Thordarson and Self*, 1993; *McLeod and Tait*, 1999; *Allen et al.*, 2002]. In contrast, during the rifting episodes of Asal-Ghoubbet (Djibouti), Krafla (Iceland) and Manda Hararo-Dabbahu, the total volume of basaltic magma emplaced in the crust was substantially larger than the volume extruded as lava flow, suggesting a more passive mechanism of rifting [e.g., *Björnsson*, 1985; *Stein et al.*, 1991]. At Krafla, activity became predominantly effusive only in the final years of the rifting episode. The modest eruptive activity associated, so far, with the current rifting episode at Manda Hararo-Dabbahu (>2 km^3 emplaced as dikes from 2005 to 2009, and probably <0.01 km^3 extruded in August 2007 [*Hamling et al.*, 2008]) suggests that the level of tectonic stress is still high and that more dikes are expected in the future. This also indicates that, in the Northern Manda Hararo Rift, the input of basaltic magma to the rift system primarily serves as a material for dike intrusion and, ultimately, crustal accretion, in close analogy with slow spreading MOR segments [e.g., *Smith and Cann*, 1999; *Dziak et al.*, 2004].

6.2. Origin of the Asymmetry Along the Northern Part of the Northern Manda Hararo Rift

[61] In a magmatic rift where successive rifting episodes occur within a laterally restricted area, normal faults can link up and grow. Cumulative deformation over a long period (at least several thousand years) creates a typical ridge-trough-ridge topography; occasional effusive magmatic activity does not modify this overall shape, but rather acts as a smoothing agent [e.g., *de Chabalier and Avouac*, 1994; *Behn et al.*, 2006]. Rift topography is well expressed in the rift south of AVC, which consists of a ~10 km wide axial depression, but it is less marked in the northern part of the Northern Manda Hararo Rift. There, faults ruptured at the top of the rift shoulder (see Figure 3 and profile N in Figure 11) [*Rowland et al.*, 2007]. In addition, during the September 2005 rifting event, more dilation occurred on the western side of the dike than on its eastern side. The population of scarps that have built the topography of the northern part of the Northern Manda Hararo Rift is also asymmetric: mapping and classification of the fault population that slipped during the Manda Hararo-Dabbahu episode has shown that most faults dip toward the west, including those with the largest offsets. Only a minority of faults dip toward the east, and most of them have a modest cumulative throw (see section 4 and Figure 3). In the northern part of the Northern Manda Hararo Rift, on the eastern side of the September 2005 dike, several westward dipping border faults are well expressed in the topography, and dip-slip motion on these faults during the rifting event is compatible with observed deformation (Figure 11). On the contrary, no fault scarp associated with a mature eastward dipping fault can be found west of the dike.

[62] Another intriguing observation is that, along the northern part of the Northern Manda Hararo Rift, the ratio between horizontal extension versus vertical throw across inferred eastward dipping faults on the western side of the September 2005 dike is larger than 1 (Figure 6). This may suggest that these inferred normal faults dip at low angle. However, this would contradict observations made at active and extinct magmatic rifts in Afar, Iceland and the Mid-Atlantic Ridge, where normal faults usually dip at a steep angle [e.g., *Brandsdóttir and Einarsson*, 1979; *Forslund and Gudmundsson*, 1991; *Stein et al.*, 1991; *Angelier and Bergerat*, 1997; *Manighetti et al.*, 1998; *Singh et al.*, 2006; *Doubre et al.*, 2007; *Rowland et al.*, 2007].

[63] In contrast, low ratios of width:throw have been reported on steep faults in the Möfell area, on the eastern side of the Krafla rift (northern Icelandic rift), about 15 km north of the Krafla caldera [*Opheim and Gudmundsson*, 1989; *Dauteuil et al.*, 2001]. In Afar, InSAR data may also suggest that current deformation in the Asal-Ghoubbet rift is controlled by two conjugate faults accommodating a quantity of horizontal extension equal to or larger than vertical motion measured across them; this effect appears to be more pronounced on the fault that has the smallest topographic expression [*Peltzer and Doubre*, 2006].

[64] It has been suggested that this peculiar kinematic behavior may be typical of the early stage of normal fault growth. In a magmatic rift, normal faults form in response to the stress field induced by the opening of a magma-filled crack at depth [*Pollard et al.*, 1983]. Large normal faults usually grow by increasing the vertical throw of preexisting tension fractures; the existence of subvertical columnar joints within the lava pile might introduce a significant weakness of the rocks when subject to horizontal extension, thus favoring a vertical direction for initial failure [*Opheim and Gudmundsson*, 1989]. However, a purely tensile stress regime may only exist at shallow depth, and a connection between superficial tensional fractures and deep magma-filled vertical cracks (the dike) via a normal fault at intermediate depth is required [*Angelier and Bergerat*, 1997; *Acocella et al.*, 2003; *Tentler*, 2005].

[65] Yet, it is not clear how the transition from a situation dominated by extensional fractures with no vertical throw, to well-developed normal faults for which the steep dip

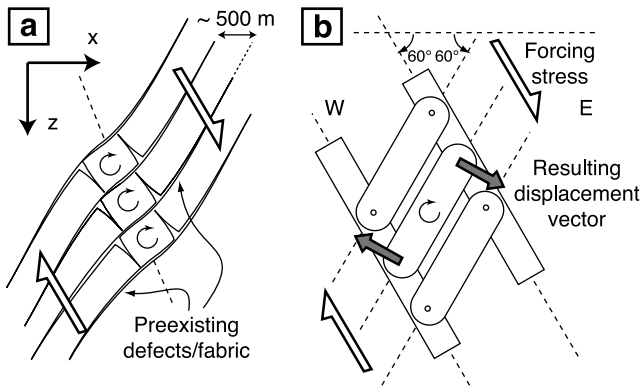

Figure 12. (a) Tentative explanation of the dilatancy resulting from shearing of a network of nonoptimally oriented normal faults (cross-section view, no vertical exaggeration). (b) Idealization of the rotating blocks as simple beams.

implies that little horizontal extension can be accommodated, is achieved. Physical model experiments of *Mastin and Pollard* [1988] provide an alternative view of the processes that occur at intermediate depths. They suggest that vertical cracks may first open, and then link up via inclined shear dislocations, thus forming a steeply dipping zone, where both mode I and mode II combine and accommodate much more extension than a single shear dislocation with the same average dip angle. Accordingly, mode I cracks involve the formation of voids. The theoretical calculations of *Gudmundsson* [1992] show that, in the Iceland rift zone, tension fractures can actually open at crustal depths of 0.5–1.5 km, before connecting and eventually forming a mature normal fault. The additional effect of pore pressure in the rocks can increase these estimates and should be taken into account because of the presence of fluid-filled voids at seismogenic depth in Afar [*Noir et al.*, 1997]. We argue that the observations presented in this paper document the incremental deformation associated with the formation of nascent normal faults on the western side of the September 2005 dike in the northern part of the Northern Manda Hararo Rift.

[66] We further propose that the observed dilation during the birth of a crustal shear zone results from an inelastic dilatancy effect similar to that reported prior to fault growth and rupture of the sample in triaxial compression experiments [*Brace et al.*, 1966]. Following the ideas of *King and Sammis* [1992], we present a conceptual model that attempts to explain the striking features of surface deformation across the northern part of the Northern Manda Hararo Rift during the September 2005 dike intrusion (Figure 12). During the initial stage of formation of a fault gouge, tensile fractures first nucleate, and induce a dilatancy of the rock mass. Rotation of the ruptured blocks/grains then occurs. This process is self similar, and the amount of dilatancy depends on the scale of the largest preexisting defects. In the laboratory, this may be the grain size. In the case of the 2005 Manda Hararo-Dabbahu rifting event, preexisting westward dipping normal faults represent barriers that must be broken to form an eastward dipping shear zone. The anisotropy caused by the presence of these large-scale defects may amplify the dilatancy involved in the growth of eastward dipping faults that connect the dike to the surface. On the eastern side of the dike, mature westward dipping faults may have slipped in a pure dip-slip fashion.

6.3. Two-Stage Rifting Scenario

[67] The location of dike emplacement at MOR can show some lateral variability, but dikes are generally observed to remain confined within the limits of the median valley [*Chadwick and Embley*, 1998; *Smith and Cann*, 1999]. The odd position of the dike with respect to the axial depression in the northern part of the Northern Manda Hararo Rift segment may thus be explained by a progressive eastward migration of the average dike location on the long term. Broad-scale interaction of the Manda Hararo Rift with nearby overlapping rifts, in particular the Alayta segment, might provide an explanation for the out-of-equilibrium state of the northern part of the Northern Manda Hararo Rift on timescales of ~1 Mya [*Tapponnier et al.*, 1990; *Manighetti et al.*, 2001]. Another possibility is that the average position of dikes is correctly indicated by the trend of the axial depression in the southern part of the Northern Manda Hararo Rift segment only, where the September 2005 dike emplaced inside the depression; in contrast, rifting in the northern part of the Northern Manda Hararo Rift segment occurred to the east of the axial graben, which is not well developed, suggesting a greater variety of lateral position of dikes in this area, possibly as a result of the interference of successive dike intrusions coming from the north (Dabbahu) and offset to the east, and coming from the south (Northern Manda Hararo) and offset to the west (Figures 3 and 11).

[68] From June 2006, dikes have been injected along the southern part of the Northern Manda Hararo segment, and a major basaltic feeder was identified in the middle of the Northern Manda Hararo Rift segment [*Ebinger et al.*, 2008; *Keir et al.*, 2008]. During these later dike intrusions, magma chambers in the Dabbahu area did not show signs of deflation [*Hamling et al.*, 2008]. This suggests that two distinct sources of magma upwelling are currently active in the Manda Hararo-Dabbahu rift system, and that both sources may have contributed to feeding the September 2005 intrusion: first, a dike fed from a deep magma reservoir below Dabbahu, was emplaced below the eastern flank of Dabbahu; then, a series of bilateral intrusions originating from a deep midsegment reservoir at ~12.30°N relieved part of the tectonic strain in the Northern Manda Hararo Rift. The apparent migration of seismic activity during dike emplacement, with a shift toward the south on 24 September 2005 [*Wright et al.*, 2006; *Ayele et al.*, 2007], may support this two-stage magma intrusion scenario.

[69] The course of events in the Da'Ure area is less clear. Identification of an accelerating inflation at Gabho prior to the September 2005 rifting event suggests that pressure in the underlying magma chamber was high at the time when rifting commenced (Figure S9). At some time during the ascent/injection of the Dabbahu dike, cracking of Gabho magma chamber probably occurred, and magma of felsic composition escaped and was emplaced at shallow depth below Da'Ure. From 24 September 2005, northward migration of the dike away from the Wal'is magma reservoir initiated, and basaltic magma came into contact with silicic

products in the Da'Ure area, leading to the eruption of 26 September 2005 [*Yirgu et al.*, 2006; *Ayele et al.*, 2007]. Complex interactions between vertically and/or horizontally migrating magma-filled cracks, pressurized magma chambers at shallow depth, and the effect of topographic load in the Dabbahu area might have resulted in the eastward offset of the dikes between Dabbahu and AVC.

7. Conclusions

[70] In this paper, in addition to InSAR, subpixel correlations of SPOT and SAR images were introduced in a geodetic inversion of the September 2005 rifting event at Manda Hararo-Dabbahu. This complementary geodetic data set shows that $\sim$1–2 km^3 of mafic magma were emplaced as a dike extending to a depth of 10 km. Faults ruptured the surface above the 65 km long dike, individualizing a subsiding keystone-like wedge of crust. On average, absolute subsidence reached 2 m between the faults, while the uplifted shoulders rose by 2 m. Simple volume balance suggests that (1) material withdrawn from the Dabbahu and Gabho magma chambers has fed a shallow dike centered on the Da'Ure eruptive vent and (2) the dikes intruded along the Northern Manda Hararo Rift segment may have been sourced from a distinct magma reservoir. Subsequent smaller rifting events occurring in the following years with a $\sim$2–4 months periodicity strongly suggest the presence of a midsegment magma reservoir at depth greater than 10 km. Assuming that this latter magma reservoir deflated simultaneously to dike intrusion in September 2005, elastic modeling predicts a broad subsidence that would be superimposed on the deformation caused by dike opening and fault slip at shallower depth; this effect, although probable, is virtually undetectable with our data set. Taking this deflation into account increases from $\sim$1.5 m to $\sim$5 m the amount of opening predicted by our inversions for the dike near its center, and highlights the large uncertainties in the opening distribution at depth in geodetic inversions of rifting events.

[71] In the sector located between the deflating magma chambers in the Dabbahu area and the suspected midsegment magma reservoir, slip on faults is asymmetric, with a substantial amount of dilation occurring on the western side of the dike. This occurs where the dike is offset to the east with respect to the axial topographic depression, and is interpreted to result from dike injection below a mechanically anisotropic brittle crust.

[72] On the basis of these observations, a two-stage scenario for the September 2005 dike intrusion is presented. We suggest that magma originating from a deep reservoir below Dabbahu volcano was first intruded into a dike below the eastern flank of Dabbahu volcano. This pulse of magma may have triggered the current rifting episode in the Northern Manda Hararo Rift, which is fed by a deep magma reservoir located at the center of the segment, similar to the process thought to occur at MOR. Complex interaction between ascending mafic magma and preexisting silicic chambers at Da'Ure may explain the eruption of silicic products coeval to dike intrusion.

[73] The large volume of magma involved in the September 2005 Manda Hararo-Dabbahu rifting event ($\sim$1–2 km^3) is twice the cumulative volume of dikes intruded at Krafla (Iceland) from 1975 to 1984, and more than 5 times the volume of the dikes emplaced in 1978 at Asal-Ghoubbet (Djibouti) in 1978. It suggests a large tectonic stress at the onset of rifting, probably resulting from a long recurrence time (>250 years). The thickness of the crust, and the absence of a midsegment magma chamber at shallow depth may indicate that the brittle lithosphere is stronger at Northern Manda Hararo than at more evolved magmatic segments of the Krafla rift, Asal-Ghoubbet rift and at slow spreading MOR. The occurrence of more rifting events in 2006–2009 implies that the tectonic stress was not fully relieved by the 2005 rifting event, suggesting a limited magma availability at the onset of the rifting episode.

[74] **Acknowledgments.** We thank the European Space Agency (ESA) for programming the Envisat satellite and providing data crucial to this work (AOE-720). SPOT data were acquired through "Incentive for the Scientific use of Images from the SPOT system" of Centre National des Etudes Spatiales (ISIS 0607-901). The acquisition of the Quickbird images was possible thanks to support from Bonus Qualité Recherche (BQR) of IPGP. The Repeat Orbit Interferometry Package (ROI_PAC) software was provided by Caltech/Jet Propulsion Laboratory (JPL). Most figures were prepared with the Generic Mapping Tool (GMT) software by *Wessel and Smith* [1991]. We thank Cynthia Ebinger, Roger Buck, and an anonymous associate editor for their useful comments on the manuscript. This work benefited from discussions with Atalay Ayele, Eric Calais, Mathilde Cannat, Marie-Pierre Doin, Cécile Doubre, Mark Simons, and Tim Wright. This is IPGP contribution number 2512.

References

Abdallah, A., V. Courtillot, M. Kasser, A.-Y. Le Dain, J.-C. Lépine, B. Robineau, J.-C. Ruegg, P. Tapponnier, and A. Tarantola (1979), Relevance of Afar seismicity and volcanism to the mechanics of accreting plate boundaries, *Nature*, *282*, 17–23, doi:10.1038/282017a0.

Acocella, V., T. Korme, and F. Salvini (2003), Formation of normal faults along the axial zone of the Ethiopian Rift, *J. Struct. Geol.*, *25*, 503–513, doi:10.1016/S0191-8141(02)00047-0.

Allard, P., and H. Tazieff (1979), Observations of seafloor spreading in Afar during the November 1978 fissure eruption, *Nature*, *279*, 30–33, doi:10.1038/279030a0.

Allen, R. M., et al. (2002), Plume-driven plumbing and crustal formation in Iceland, *J. Geophys. Res.*, *107*(B8), 2163, doi:10.1029/2001JB000584.

Angelier, J., and F. Bergerat (1997), Effective tension-shear relationships in extensional fissure swarms, axial rift zone of northeastern Iceland, *J. Struct. Geol.*, *19*, 673–685, doi:10.1016/S0191-8141(96)00106-X.

Arnott, S. K., and G. R. Foulger (1994), The Krafla spreading segment, Iceland: 2. The accretionary stress cycle and nonshear earthquake focal mechanisms, *J. Geophys. Res.*, *99*, 23,827–23,842, doi:10.1029/94JB00688.

Audin, L. (1999), Pénétration de la dorsale d'Aden dans la dépression Afar entre 20 et 4 Ma, Ph.D. thesis, Inst. de Phys. du Globe de Paris, Paris.

Audin, L., I. Manighetti, P. Tapponnier, F. Métivier, E. Jacques, and P. Huchon (2001), Fault propagation and climatic control of sedimentation on the Ghoubbet Rift floor: Insights from the Tadjouraden cruise in the western Gulf of Aden, *Geophys. J. Int.*, *144*, 391–413, doi:10.1046/j.0956-540X.2000.01322.x.

Ayele, A., E. Jacques, M. Kassim, T. Kidane, A. Omar, S. Tait, A. Nercessian, J.-B. de Chabalier, and G. C. P. King (2007), The volcano seismic crisis in Afar, Ethiopia, starting September 2005, *Earth. Planet. Sci. Lett.*, *255*, 177–187, doi:10.1016/j.epsl.2006.12.014.

Barberi, F., and R. Santacroce (1980), The Afar Stratoid Series and the magmatic evolution of East African Rift System, *Bull. Soc. Geol. Fr.*, *22*, 891–899.

Barberi, F., S. Borsi, G. Ferrara, G. Marinelli, R. Santacroce, H. Tazieff, and J. Varet (1972a), Evolution of the Danakil depression (Afar, Ethiopia) in light of radiometric age determinations, *J. Geol.*, *80*, 720–729.

Barberi, F., H. Tazieff, and J. Varet (1972b), Volcanism in the Afar depression: Its tectonic and magmatic significance, *Tectonophysics*, *15*, 59–64, doi:10.1016/0040-1951(72)90051-0.

Barberi, F., R. Santacroce, and J. Varet (1974), Silicic peralkaline volcanic rocks of the afar depression (Ethiopia), *Bull. Volcanol.*, *38*, 755–790, doi:10.1007/BF02596907.

Barberi, F., G. Ferrara, R. Santacroce, M. Treuil, and J. Varet (1975), A transitional basalt-pantellerite sequence of fractional crystallisation, the Boina centre (Afar Rift, Ethiopia), *J. Petrol.*, *16*, 22–56.

Behn, M. D., W. R. Buck, and I. S. Sacks (2006), Topographic controls on dike injection in volcanic rift zones, *Earth. Planet. Sci. Lett.*, *246*, 188–196, doi:10.1016/j.epsl.2006.04.005.

Ben-Menahem, A., and S. J. Singh (1981), *Seismic Waves and Sources*, Springer, New York.

Bilham, R., R. Bendick, K. Larson, P. Mohr, J. Braun, S. Tesfaye, and L. Asfaw (1999), Secular and tidal strain across the main Ethiopian rift, *Geophys. Res. Lett.*, *26*, 2789–2792, doi:10.1029/1998GL005315.

Björnsson, A. (1985), Dynamics of crustal rifting in NE Iceland, *J. Geophys. Res.*, *90*, 10,151–10,162.

Björnsson, A., G. Johnsen, S. Sigurdsson, G. Thorbergsson, and E. Tryggvason (1979), Rifting of the plate boundary in North Iceland 1975–1978, *J. Geophys. Res.*, *84*, 3029–3038.

Bosworth, W., P. Huchon, and K. McClay (2005), The Red Sea and Gulf of Aden Basins, *J. Afr. Earth Sci.*, *43*, 334–378, doi:10.1016/j.jafrearsci.2005.07.020.

Brace, W. F., B. W. Paulding Jr., and C. Scholz (1966), Dilatancy in the Fracture of Crystalline Rocks, *J. Geophys. Res.*, *71*, 3939–3953.

Brandsdóttir, B., and P. Einarsson (1979), Seismic activity associated with the September 1977 deflation of the Krafla central volcano in northeastern Iceland, *J. Volcanol. Geotherm. Res.*, *6*, 197–212.

Bruce, P. M., and H. E. Huppert (1989), Thermal control of basaltic fissure eruptions, *Nature*, *342*, 665–667, doi:10.1038/342665a0.

Buck, W. R. (2006), The role of magma in the development of the Afro-Arabian Rift System, in *The Afar Volcanic Province Within the East African Rift System*, edited by G. Yirgu, C. J. Ebinger, and P. K. H. Maguire, *Geol. Soc. Spec. Publ. London*, *259*, 43–54, doi:10.1144/GSL.SP.2006.259.01.05.

Buck, W. R., P. Einarsson, and B. Brandsdóttir (2006), Tectonic stress and magma chamber size as controls on dike propagation: Constraints from the 1975–1984 Krafla rifting episode, *J. Geophys. Res.*, *111*, B12404, doi:10.1029/2005JB003879.

Burke, K., and J. F. Dewey (1973), Plume-generated triple junctions: Key indicators in applying plate tectonics to old rocks, *J. Geol.*, *81*, 406–433.

Chadwick, W. W., and R. W. Embley (1998), Graben formation associated with recent dike intrusions and volcanic eruptions on the mid-ocean ridge, *J. Geophys. Res.*, *103*, 9807–9826, doi:10.1029/97JB02485.

Chu, D., and R. G. Gordon (1998), Current plate motions across the Red Sea, *Geophys. J. Int.*, *135*, 313–328, doi:10.1046/j.1365-246X.1998.00658.x.

Chu, D., and R. G. Gordon (1999), Evidence for motion between Nubia and Somalia along the Southwest Indian ridge, *Nature*, *398*, 64–67, doi:10.1038/18014.

CNR-CNRS Afar Team (1973), Geology of northern Afar (Ethiopia), *Rev. Geogr. Phys. Geol. Dyn.*, *2*, 442–490.

Cochran, J. R. (1981), The Gulf of Aden: Structure and evolution of a young ocean basin and continental margin, *J. Geophys. Res.*, *86*, 263–287.

Courtillot, V. (1982), Propagating rifts and continental breakup, *Tectonics*, *1*, 239–250, doi:10.1029/TC001i003p00239.

Courtillot, V., F. Landre, J. Achache, N. Bonhommet, R. Montigny, and G. Féraud (1984), Episodic spreading and rift propagation: New paleomagnetic and geochronologic data from the afar Nascent passive margin, *J. Geophys. Res.*, *89*, 3315–3334.

Crouch, S. L., and A. M. Starfield (1983), *Boundary Element Methods in Solid Mechanics*, Allen and Unwin, London.

Dauteuil, O., J. Angelier, F. Bergerat, S. Verrier, and T. Villemin (2001), Deformation partitioning inside a fissure swarm of the northern Iceland Rift, *J. Struct. Geol.*, *23*, 1359–1372, doi:10.1016/S0191-8141(01)00002-5.

de Chabalier, J.-B., and J.-P. Avouac (1994), Kinematics of the Asal Rift (Djibouti) determined from the deformation of Fieale volcano, *Science*, *265*, 1677–1681.

Demets, C., R. G. Gordon, D. F. Argus, and S. Stein (1994), Effect of recent revisions to the geomagnetic reversal timescale on estimates of current plate motions, *Geophys. Res. Lett.*, *21*, 2191–2194.

Deniel, C., P. Vidal, C. Coulon, P.-J. Vellutini, and P. Piguet (1994), Temporal evolution of mantle sources during continental rifting: The volcanism of Djibouti (Afar), *J. Geophys. Res.*, *99*, 2853–2869.

Dominguez, S., J.-P. Avouac, and R. Michel (2003), Horizontal coseismic deformation of the 1999 Chi-Chi earthquake measured from SPOT satellite images: Implications for the seismic cycle along the western foothills of central Taiwan, *J. Geophys. Res.*, *108*(B2), 2083, doi:10.1029/2001JB000951.

Doubre, C., and G. Peltzer (2007), Fluid-controlled faulting process in the Asal Rift, Djibouti, from 8 yr of radar interferometry observations, *Geology*, *35*, 69–72, doi:10.1130/G23022A.1.

Doubre, C., I. Manighetti, C. Dorbath, L. Dorbath, E. Jacques, and J.-C. Delmond (2007), Crustal structure and magmato-tectonic processes in an active rift (Asal-Ghoubbet, Afar, East Africa): 1. Insights from a 5-month seismological experiment, *J. Geophys. Res.*, *112*(B11), B05405, doi:10.1029/2005JB003940.

Du, Y., and A. Aydin (1992), Three-dimensional characteristics of dike intrusion along the northern Iceland Rift from inversion of geodetic data, *Tectonophysics*, *204*, 111–121.

Dunn, R. A., V. Lekiæ, R. S. Detrick, and D. R. Toomey (2005), Three-dimensional seismic structure of the Mid-Atlantic Ridge (35°N): Evidence for focused melt supply and lower crustal dike injection, *J. Geophys. Res.*, *110*, B09101, doi:10.1029/2004JB003473.

Dziak, R. P., D. K. Smith, D. R. Bohnenstiehl, C. G. Fox, D. Desbruyeres, H. Matsumoto, M. Tolstoy, and D. J. Fornari (2004), Evidence of a recent magma dike intrusion at the slow spreading Lucky Strike segment, Mid-Atlantic Ridge, *J. Geophys. Res.*, *109*(B18), B12102, doi:10.1029/2004JB003141.

Dziak, R. P., D. R. Bohnenstiehl, J. P. Cowen, E. T. Baker, K. H. Rubin, J. H. Haxel, and M. J. Fowler (2007), Rapid dike emplacement leads to eruptions and hydrothermal plume release during seafloor spreading events, *Geology*, *35*, 579–582.

Dziewonski, A. M., T.-A. Chou, and J. H. Woodhouse (1981), Determination of earthquake source parameters from waveform data for studies of global and regional seismicity, *J. Geophys. Res.*, *86*, 2825–2852.

Dziewonski, A. M., G. Ekström, J. E. Franzen, and J. H. Woodhouse (1987), Centroid-moment tensor solutions for January–March 1986, *Phys. Earth Planet. Inter.*, *45*, 1–10, doi:10.1016/0031-9201(87)90193-2.

Ebinger, C. J., and M. Casey (2001), Continental breakup in magmatic provinces: An Ethiopian example, *Geology*, *29*, 527–530, doi:10.1130/0091-7613(2001)029<0527:CBIMPA>2.0.CO;2.

Ebinger, C. J., and N. J. Hayward (1996), Soft plates and hot spots: Views from Afar, *J. Geophys. Res.*, *101*, 21,859–21,876, doi:10.1029/96JB02118.

Ebinger, C. J., and N. H. Sleep (1998), Cenozoic magmatism throughout East Africa resulting from impact of a single plume, *Nature*, *395*, 788–791, doi:10.1038/27417.

Ebinger, C. J., D. Keir, A. Ayele, E. Calais, T. J. Wright, M. Belachew, J. O. S. Hammond, E. Campbell, and W. R. Buck (2008), Capturing magma intrusion and faulting processes during continental rupture: Seismicity of the Dabbahu (Afar) rift, *Geophys. J. Int.*, *174*, 1138–1152, doi:10.111/j.1365-246X.2008.03877.x.

Einarsson, P., and B. Brandsdóttir (1980), Seismological evidence for lateral magma intrusion during the July 1978 deflation of the Krafla volcano in NE-Iceland, *J. Geophys. Res.*, *47*, 160–165.

Fialko, Y. A., and A. M. Rubin (1998), Thermodynamics of lateral dike propagation: Implications for crustal accretion at slow spreading mid-ocean ridges, *J. Geophys. Res.*, *103*, 2501–2514, doi:10.1029/97JB03105.

Fialko, Y., Y. Khazan, and M. Simons (2001), Deformation due to a pressurized horizontal circular crack in an elastic half-space, with applications to volcano geodesy, *Geophys. J. Int.*, *146*, 181–190.

Forslund, T., and A. Gudmundsson (1991), Crustal spreading due to dikes and faults in southwest Iceland, *J. Struct. Geol.*, *13*, 443–457, doi:10.1016/0191-8141(91)90017-D.

Gouin, P. (1979), *Earthquake History of Ethiopia and the Horn of Africa*, Int. Dev. Res. Cent., Ottawa, Ont., London.

Gràcia, E., D. Bideau, R. Hekinian, and Y. Lagabrielle (1999), Detailed geological mapping of two contrasting second-order segments of the Mid-Atlantic Ridge between Oceanographer and Hayes fracture zones (33°30′N–35°N), *J. Geophys. Res.*, *104*, 22,903–22,922, doi:10.1029/1999JB900161.

Gudmundsson, A. (1986), Formation of crustal magma chambers in Iceland, *Geology*, *14*, 164–166, doi:10.1130/0091-7613(1986)14.

Gudmundsson, A. (1987), Formation and mechanics of magma reservoirs in Iceland, *Geophys. J. Int.*, *91*, 27–41, doi:10.1111/j.1365-246X.1987.tb05211.x.

Gudmundsson, A. (1990), Emplacement of dikes, sills and crustal magma chambers at divergent plate boundaries, *Tectonophysics*, *176*, 257–275, doi:10.1016/0040-1951(90)90073-H.

Gudmundsson, A. (1992), Formation and growth of normal faults at the divergent plate boundary in Icleland, *Terra Nova*, *4*, 464–471.

Hamling, I. J., A. Ayele, L. Bennati, E. Calais, C. J. Ebinger, D. Keir, E. Lewi, T. J. Wright, and G. Yirgu (2008), Geodetic observations of the ongoing Dabbahu rifting episode: New dyke intrusions in 2006 and 2007, *Geophys. J. Int.*, *178*, 989–1003, doi:10.1111/j.1365-246X.2009.04163.x.

Hanks, T. C., and H. Kanamori (1979), A moment magnitude scale, *J. Geophys. Res.*, *84*, 2348–2350.

Hayward, N. J., and C. J. Ebinger (1996), Variations in the along-axis segmentation of the Afar Rift System, *Tectonics*, *15*, 244–257, doi:10.1029/95TC02292.

Ida, Y. (1999), Effects of the crustal stress on the growth of dikes: Conditions of intrusion and extrusion of magma, *J. Geophys. Res.*, *104*, 17,897–17,910, doi:10.1029/1998JB900040.

Jacques, E., J.-C. Ruegg, J.-C. Lépine, P. Tapponnier, G. C. P. King, and A. Omar (1999), Relocation of M $\geq$ 2 events of the 1989 Dôbi seismic sequence in Afar: Evidence for earthquake migration, *Geophys. J. Int.*, *138*, 447–469, doi:10.1046/j.1365-246X.1999.00881.x.

Jestin, F., P. Huchon, and J. M. Gaulier (1994), The Somalia plate and the East African Rift System: Present-day kinematics, *Geophys. J. Int.*, *116*, 637–654, doi:10.1111/j.1365-246X.1994.tb03286.x.

Jónsson, S., H. Zebker, P. Segall, and F. Amelung (2002), Fault slip distribution of the 1999 M_w 7.1 Hector Mine, California, earthquake, estimated from satellite radar and GPS measurements, *Bull. Seismol. Soc. Am.*, *92*, 1377–1389, doi:10.1785/0120000922.

Kebede, F., and O. Kulhánek (1989), Dynamic source parameters of the March–May 1969 Serdo earthquake sequence in central Afar, Ethiopia, deduced from teleseismic body waves, *J. Geophys. Res.*, *94*, 5603–5614.

Keir, D., et al. (2008), Evidence for focused magmatic accretion at segment centers from lateral dike injections captured beneath the Red Sea rift in Afar, *Geology*, *37*, 59–62, doi:10.1130/G25147A.1.

Kidane, T., V. Courtillot, I. Manighetti, L. Audin, P. Lahitte, X. Quidelleur, P.-Y. Gillot, Y. Gallet, J. Carlut, and T. Haile (2003), New paleomagnetic and geochronologic results from Ethiopian Afar: Block rotations linked to rift overlap and propagation and determination of a ~2 Ma reference pole for stable Africa, *J. Geophys. Res.*, *108*(B2), 2102, doi:10.1029/2001JB000645.

King, G. C. P. (1978), Geological faults: Fracture, creep and strain, *Philos. Trans. R. Soc. London, Ser. A*, *288*, 197–212.

King, G. C. P., and M. Cocco (2001), Fault interaction by elastic stress changes: New clues from earthquake sequences, *Adv. Geophys.*, *44*, 1–38.

King, G. C. P., and C. G. Sammis (1992), The mechanisms of finite brittle strain, *Pure Appl. Geophys.*, *138*(4), 611–640, doi:10.1007/BF00876341.

King, G. C. P., R. S. Stein, and J. Lin (1994), Static stress changes and the triggering of earthquakes, *Bull. Seismol. Soc. Am.*, *92*, 1377–1389, doi:10.1785/0120000922.

Klinger, Y., R. Michel, and G. C. P. King (2006), Evidence for an earthquake barrier model from Mw ~ 7.8 Kokoxili (Tibet) earthquake slip-distribution, *Earth. Planet. Sci. Lett.*, *242*, 354–364, doi:10.1016/j.epsl.2005.12.003.

Knopoff, L., and M. J. Randall (1970), The compensated linear-vector dipole: A possible mechanism for deep earthquakes, *J. Geophys. Res.*, *75*, 4957–4963, doi:10.1029/JB075i026p04957.

Lahitte, P., P.-Y. Gillot, and V. Courtillot (2003a), Silicic central volcanoes as precursors to rift propagation: The Afar case, *Earth. Planet. Sci. Lett.*, *207*, 103–116, doi:10.1016/S0012-821X(02)01130-5.

Lahitte, P., P.-Y. Gillot, T. Kidane, V. Courtillot, and A. Bekele (2003b), New age constraints on the timing of volcanism in central Afar, in the presence of propagating rifts, *J. Geophys. Res.*, *108*(B2), 2123, doi:10.1029/2001JB001689.

Le Dain, A.-Y., B. Robineau, and P. Tapponnier (1980), Les effets tectoniques de l'événement sismique et magmatique de Novembre 1978 dans le rift d'Asal-Ghoubbet, *Bull. Soc. Geol. Fr.*, *22*, 817–822.

Lépine, J.-C., J.-C. Ruegg, and A. M. Anis (1980), Les effets tectoniques de l'événement sismique et magmatique de Novembre 1978 dans le rift d'Asal-Ghoubbet, *Bull. Soc. Geol. Fr.*, *22*, 809–816.

Leprince, S., S. Barbot, F. Ayoub, and J.-P. Avouac (2007), Automatic and precise orthorectification, coregistration, and subpixel correlation of satellite images, application to ground deformation measurements, *IEEE Trans. Geosci. Remote Sens.*, *45*, 1529–1558, doi:10.1109/TGRS.2006.888937.

Leroy, J., et al. (2004), From rifting to spreading in the eastern Gulf of Aden: A geophysical survey of a young oceanic basin from margin to margin, *Terra Nova*, *16*, 185–192, doi:doi:10.1111/j.1365-3121.2004.00550.x.

Lin, J., and E. M. Parmentier (1990), A finite amplitude necking model of rifling in brittle lithosphere, *J. Geophys. Res.*, *95*, 4909–4923.

Lin, J., G. M. Purdy, H. Schouten, J.-C. Sempere, and C. Zervas (1990), Evidence from gravity data for focused magmatic accretion along the Mid-Atlantic Ridge, *Nature*, *344*, 627–632, doi:10.1038/344627a0.

Lister, J. R., and R. C. Kerr (1991), Fluid-mechanical models of crack propagation and their application to magma transport in dykes, *J. Geophys. Res.*, *96*, 10,049–10,077.

Lohman, R. B., and M. Simons (2005), Some thoughts on the use of InSAR data to constrain models of surface deformation: Noise structure and data downsampling, *Geochem. Geophys. Geosyst.*, *6*, Q01007, doi:10.1029/2004GC000841.

Manighetti, I., P. Tapponnier, V. Courtillot, S. Gruszow, and P.-Y. Gillot (1997), Propagation of rifting along the Arabia-Somalia plate boundary: The Gulfs of Aden and Tadjoura, *J. Geophys. Res.*, *102*, 2681–2710, doi:10.1029/96JB01185.

Manighetti, I., P. Tapponnier, P.-Y. Gillot, E. Jacques, V. Courtillot, R. Armijo, J.-C. Ruegg, and G. C. P. King (1998), Propagation of rifting along the Arabia-Somalia plate boundary: Into Afar, *J. Geophys. Res.*, *103*, 4947–4974, doi:10.1029/97JB02758.

Manighetti, I., P. Tapponnier, V. Courtillot, Y. Gallet, E. Jacques, and P.-Y. Gillot (2001), Strain transfer between disconnected, propagating rifts in Afar, *J. Geophys. Res.*, *106*, 13,613–13,666, doi:10.1029/2000JB900454.

Mastin, L. G., and D. D. Pollard (1988), Surface deformation and shallow dike intrusion processes at Inyo craters, Long Valley, California, *J. Geophys. Res.*, *93*, 13,221–13,235.

McClusky, S., R. Reilinger, S. Mahmoud, D. Ben Sari, and A. Tealeb (2003), GPS constraints on Africa (Nubia) and Arabia plate motions, *Geophys. J. Int.*, *155*, 126–138, doi:10.1046/j.1365-246X.2003.02023.x.

McKenzie, D. P., and D. Davies (1970), Plate tectonics of the Red Sea and East Africa, *Nature*, *226*, 243–248, doi:10.1038/226243a0.

McLeod, P., and S. Tait (1999), The growth of dykes from magma chambers, *J. Volcanol. Geotherm. Res.*, *92*, 231–245, doi:10.1016/S0377-0273(99)00053-0.

Menke, W. (1989), *Geophysical Data Analysis: Discrete Inverse Theory*, rev. ed., Academic, New York.

Michel, R., and J.-P. Avouac (2002), Deformation due to the 17 August 1999 Izmit, Turkey, earthquake measured from SPOT images, *J. Geophys. Res.*, *107*(B4), 2062, doi:10.1029/2000JB000102.

Michel, R., J.-P. Avouac, and J. Taboury (1999a), Measuring ground displacements from SAR amplitude images: Application to the Landers earthquake, *Geophys. Res. Lett.*, *26*, 875–878, doi:10.1029/1999GL900138.

Michel, R., J.-P. Avouac, and J. Taboury (1999b), Measuring near field coseismic displacements from SAR images: Application to the Landers earthquake, *Geophys. Res. Lett.*, *26*, 3017–3020, doi:10.1029/1999GL900524.

Mogi, K. (1958), Relations between the eruptions of various volcanoes and the deformations of the ground surfaces around them, *Bull. Earthquake Res. Inst. Univ. Tokyo*, *36*, 99–134.

Mohr, P. A. (1970), The Afar triple junction and sea-floor spreading, *J. Geophys. Res.*, *75*, 7340–7352, doi:10.1029/JB075i035p07340.

Mohr, P. (1978), Present-day strain rates at the northern end of the Ethiopian rift valley, *Tectonophysics*, *44*, 141–160, doi:10.1016/0040-1951(78)90067-7.

Noir, J., E. Jacques, S. Békri, P. M. Adler, P. Tapponnier, and G. C. P. King (1997), Fluid flow triggered migration of events in the 1989 Dobi earthquake sequence of central Afar, *Geophys. Res. Lett.*, *24*, 2335–2338, doi:10.1029/97GL02182.

Okada, Y. (1985), Surface deformation to shear and tensile faults in a half space, *Bull. Seismol. Soc. Am.*, *75*, 1135–1154.

Opheim, J. A., and A. Gudmundsson (1989), Formation and geometry of fractures, and related volcanism, of the Krafla fissure swarm, northeast Iceland, *Geol. Soc. Am. Bull*, *101*, 1608–1622.

Parsons, T., and G. A. Thompson (1991), The role of magma overpressure in suppressing earthquakes and topography: Worldwide examples, *Science*, *253*, 1399–1402, doi:10.1126/science.253.5026.1399.

Peltzer, G., and C. Doubre (2006), Asymmetric opening and episodic faulting in the Asal Rift, Djibouti, *Alaska Satell. Facil. Newsl.*, *3*, 2–3.

Pollard, D. D., P. T. Delaney, W. A. Duffield, E. T. Endo, and A. T. Okamura (1983), Surface deformation in volcanic rift zones, *Tectonophysics*, *94*, 541–584, doi:10.1016/0040-1951(83)90034-3.

Qin, R., and W. R. Buck (2008), Why meter-wide dikes at oceanic spreading centers?, *Earth. Planet. Sci. Lett.*, *265*, 466–474, doi:10.1016/j.epsl.2007.10.044.

Rabain, A., M. Cannat, J. Escartín, G. Pouliquen, C. Deplus, and C. Rommevaux-Jestin (2001), Focused volcanism and growth of a slow spreading segment (Mid-Atlantic Ridge, 35°N), *Earth. Planet. Sci. Lett.*, *185*, 211–224, doi:10.1016/S0012-821X(00)00371-X.

Rosen, P. A., S. Henley, G. Peltzer, and M. Simons (2004), Updated repeat orbit interferometry package released, *Eos Trans. AGU*, *85*, 47, doi:10.1029/2004EO050004.

Rowland, J. V., E. Baker, C. J. Ebinger, D. Keir, T. Kidane, J. Biggs, N. Hayward, and T. J. Wright (2007), Fault growth at a nascent slow-spreading ridge: 2005 Dabbahu rifting episode, Afar, *Geophys. J. Int.*, *171*, 1226–1246, doi:10.1111/j.1365-246X.2007.03584.x.

Rubin, A. M. (1992), Dike-induced faulting and graben subsidence in volcanic rift zones, *J. Geophys. Res.*, *97*, 1839–1858.

Rubin, A. M., and D. Gillard (1998), Dike-induced earthquakes: Theoretical considerations, *J. Geophys. Res.*, *103*, 10,017–10,030, doi:10.1029/97JB03514.

Rubin, A. M., and D. D. Pollard (1988), Dike-induced faulting in rift zones of Iceland and Afar, *Geology*, *16*, 413–417, doi:10.1130/0091-7613(1988)016<0413:DIFIRZ>2.3.CO;2.

Ruegg, J.-C., M. Kasser, J.-C. Lépine, and A. Tarantola (1979), Geodetic measurements of rifting associated with a seismo-volcanic crisis in afar, *Geophys. Res. Lett.*, *6*, 817–820.

Ruegg, J. C., P. Briole, K. L. Feigl, A. Orsoni, C. Vigny, M. A. Abdallah, O. Bellier, J.-B. de Chabalier, P. Huchon, and E. Jacques (1993), First epoch geodetic GPS measurements across the Afar plate boundary zone, *Geophys. Res. Lett.*, *20*, 1899–1902.

Schilling, J.-G., R. H. Kingsley, B. B. Hanan, and B. L. McCully (1992), Nd-Sr-Pb isotopic variations along the Gulf of Aden: Evidence for Afar mantle plume-continental lithosphere interaction, *J. Geophys. Res.*, *97*, 10,927–10,926, doi:10.1029/92JB00415.

Sigmarssson, O., M. Condomines, K. Grönvold, and T. Thordarson (1991), Extreme magma homogeneity in the 1783–84 Lakagigar eruption: Origin of a large volume of evolved basalt in Iceland, *Geophys. Res. Lett.*, *18*, 2229–2232, doi:10.1029/91GL02328.

Sigurdsson, H., and R. S. J. Sparks (1978), Rifting episode in north Iceland in 1874–1875 and the eruptions of Askja and Sveinagja, *Bull. Volcanol.*, *41*, 149–167, doi:10.1007/BF02597219.

Simons, M., Y. Fialko, and L. Rivera (2002), Coseismic deformation from the 1999 M_w 7.1 Hector Mine, California, earthquake as inferred from InSAR and GPS observations, *Bull. Seismol. Soc. Am.*, *92*, 1390–1402, doi:10.1785/0120000933.

Singh, S. C., W. C. Crawford, H. Carton, T. Seher, V. Combier, M. Cannat, J. Pablo Canales, D. Düsünür, J. Escartin, and J. Miguel Miranda (2006), Discovery of a magma chamber and faults beneath a Mid-Atlantic Ridge hydrothermal field, *Nature*, *442*, 1029–1032, doi:10.1038/nature05105.

Smith, D. K., and J. R. Cann (1999), Constructing the upper crust of the Mid-Atlantic Ridge: A reinterpretation based on the Puna Ridge, Kilauea Volcano, *J. Geophys. Res.*, *104*, 25,379–25,400, doi:10.1029/1999JB900177.

Solomon, S. C., P. Y. Huang, and L. Meinke (1988), The seismic moment budget of slowly spreading ridges, *Nature*, *334*, 58–60, doi:10.1038/334058a0.

Spence, D. A., and D. L. Turcotte (1985), Magma-driven propagation of cracks, *J. Geophys. Res.*, *90*, 575–580, doi:10.1029/JB090iB01p00575.

Stein, R. S., P. Briole, J.-C. Ruegg, P. Tapponnier, and F. Gasse (1991), Contemporary, Holocene, and quaternary deformation of the Asal Rift, Djibouti: Implications for the mechanics of slow spreading ridges, *J. Geophys. Res.*, *96*, 21,789–21,806.

Stieltjes, L. (1980), Carte géologique du Rift d'Asal, République de Djibouti (Dépression Afar, Est-africain), scale, 1:50000, Cent. Natl. de la Rech. Sci., Paris.

Sykes, L. R. (1970), Earthquake swarms and sea-floor spreading, *J. Geophys. Res.*, *75*, 6598–6611, doi:10.1029/JB075i032p06598.

Takada, A. (1989), Magma transport and reservoir formation by a system of propagating cracks, *Bull. Volcanol.*, *52*, 118–126, doi:10.1007/BF00301551.

Tapponnier, P., and J. Francheteau (1978), Necking of the lithosphere and the mechanics of slowly accreting plate boundaries, *J. Geophys. Res.*, *83*, 3955–3970.

Tapponnier, P., R. Armijo, I. Manighetti, and V. Courtillot (1990), Bookshelf faulting and horizontal block rotations between overlapping rifts in southern Afar, *Geophys. Res. Lett.*, *17*, 1–4.

Tarantola, A., and B. Valette (1982), Generalized nonlinear inverse problems solved using the least squares criterion, *Rev. Geophys.*, *20*, 219–232.

Tarantola, A., J.-C. Ruegg, and J.-C. Lépine (1979), Geodetic evidence for rifting in Afar: A brittle-elastic model of the behaviour of the lithosphere, *Earth. Planet. Sci. Lett.*, *45*, 435–444, doi:10.1016/0012-821X(79)90142-0.

Tazieff, H., J. Varet, F. Barberi, and G. Giglia (1972), Tectonic significance of the Afar (or Danakil) Depression, *Nature*, *235*, 144–147, doi:10.1038/235144a0.

Tentler, T. (2005), Propagation of brittle failure triggered by magma in Iceland, *Tectonophysics*, *406*, 17–38, doi:10.1016/j.tecto.2005.05.016.

Thordarson, T., and S. Self (1993), The Laki (Skaftár Fires) and Grímsvötn eruptions in 1783–1785, *Bull. Volcanol.*, *55*, 233–263, doi:10.1007/BF00624353.

Tryggvason, E. (1984), Widening of the Krafla fissure swarm during the 1975–1981 volcano-tectonic episode, *Bull. Volcanol.*, *47*, 47–69, doi:10.1007/BF01960540.

Tryggvason, E. (1986), Multiple magma reservoirs in a rift zone volcano: Ground deformation and magma transport during the September 1984 eruption of Krafla, Iceland, *J. Volcanol. Geotherm. Res.*, *28*, 1–44, doi:10.1016/0377-0273(86)90003-X.

Van Puymbroeck, N., R. Michel, R. Binet, J.-P. Avouac, and J. Taboury (2000), Measuring earthquakes from optical satellite images, *Appl. Opt.*, *39*, 3486–3494.

Varet, J. (1975), Geological map of central Afar, Cent. Natl. de la Rech. Sci., Paris.

Vigny, C., P. Huchon, J.-C. Ruegg, K. Khanbari, and L. M. Asfaw (2006), Confirmation of Arabia plate slow motion by new GPS data in Yemen, *J. Geophys. Res.*, *111*(B10), B02402, doi:10.1029/2004JB003229.

Walpersdorf, A., C. Vigny, J.-C. Ruegg, P. Huchon, L. M. Asfaw, and S. Al Kirbash (1999), 5 years of GPS observations of the Afar triplejunction area, *J. Geodyn.*, *28*, 225–236, doi:10.1016/S0264-3707(98)00039-8.

Weertman, J. (1971), Theory of water-filled crevasses in glaciers applied to vertical magma transport beneath oceanic ridges, *J. Geophys. Res.*, *76*, 1171–1183, doi:10.1029/JB076i005p01171.

Wessel, P., and W. H. F. Smith (1991), Free software helps map and display data, *Eos Trans. AGU*, *72*, 441, doi:10.1029/90EO00319.

White, R., and D. McKenzie (1989), Magmatism at rift zones: The generation of volcanic continental margins and flood basalts, *J. Geophys. Res.*, *94*, 7685–7729.

Wills, S., and W. R. Buck (1997), Stress-field rotation and rooted detachment faults: A Coulomb failure analysis, *J. Geophys. Res.*, *102*, 20,503–20,514, doi:10.1029/97JB01512.

Wolfenden, E., C. Ebinger, G. Yirgu, A. Deino, and D. Ayalew (2004), Evolution of the northern main Ethiopian rift: Birth of a triple junction, *Earth. Planet. Sci. Lett.*, *224*, 213–228, doi:10.1016/j.epsl.2004.04.022.

Wright, T. J., C. Ebinger, J. Biggs, A. Ayele, G. J. Yirgu, D. Keir, and A. Stork (2006), Magma-maintained rift segmentation at continental rupture in the 2005 Afar dyking episode, *Nature*, *442*, 291–294, doi:10.1038/nature04978.

Yirgu, G., A. Ayele, and D. Ayalew (2006), Recent seismovolcanic crisis in northern Afar, Ethiopia, *Eos Trans. AGU*, *87*, 325–329, doi:10.1029/2006EO330001.

Zumbo, V., G. Féraud, P. Vellutini, P. Piguet, and J. Vincent (1995), First $^{40}Ar/^{39}Ar$ dating on early Pliocene to Plio-Pleistocene magmatic events of the Afar, Republic of Djibouti, *J. Volcanol. Geotherm. Res.*, *65*, 281–295, doi:10.1016/0377-0273(94)00107-R.

R. Binet, Laboratoire de Détection et de Géophysique, Commisariat l'Energie Atomique, BP12, F-91680 Bruyères-le-Châtel, France.

J.-B. de Chabalier, A. Delorme, R. Grandin, E. Jacques, G. C. P. King, Y. Klinger, P. Pinzuti, A. Socquet and P. Tapponnier, Equipe de Tectonique et Mécanique de la Lithosphère, Institut de Physique du Globe de Paris, UMR 7154, CNRS, 4 place Jussieu, F-75252 Paris CEDEX 05, France. (grandin@ipgp.jussieu.fr)

C. Lasserre, Laboratoire de Géophysique Interne et Tectonophysique, Université Joseph Fourier, INSU, UMR 5559, CNRS, F-38041 Grenoble CEDEX 09, France.

S. Tait, Equipe de Dynamique des Fluides Géologiques, Institut de Physique du Globe de Paris, UMR 7154, CNRS, 4 place Jussieu, F-75252 Paris CEDEX 05, France.